Diphenylmethane Based Metallomacrocyclic Dithiocarbamate Complexes: Synthesis, Characterization and Their Binding Study Towards Environmentally Hazardous Organic Dyes

Abstract

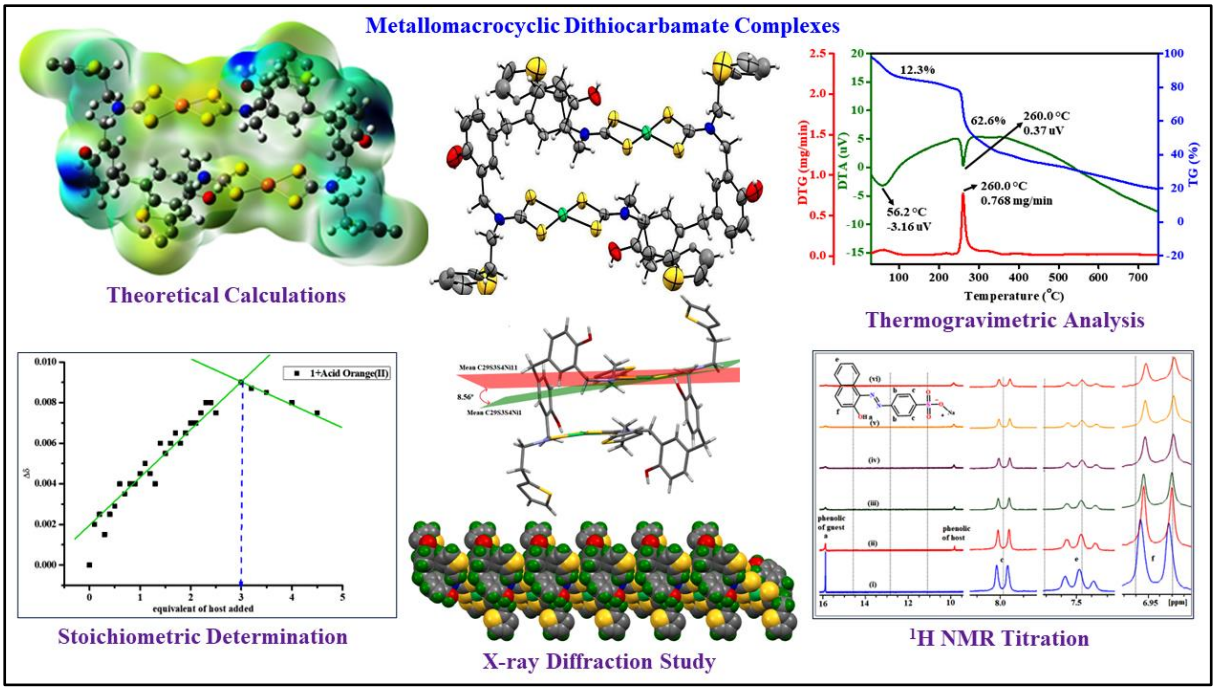

In this chapter, the secondary diamino precursors 4,4'-methylenebis-2-((2-thiophen-2-yl)ethylamino)methylphenol (**H_2L^1**) and 4,4'-methylenebis-2-(cyclohexylamino)methylphenol (**H_2L^2**) were designed and synthesized in chapter 2 have been utilized to derive a new series of 32-membered homobimetallic dithiocarbamate macrocyclic complexes [M(II)$_2$-μ^2-bis-{κ^2*S*^*S*-$S_2CN(R)CH_2C_6H_3(OH)$}$_2CH_2$] (R = 2-thiophenylethyl; Ni(II) **1**, Cu(II) **2**, Zn(II) **3;** R = cyclohexyl; Ni(II) **4**, Cu(II) **5**, Zn(II) **6**). A number of analytical tools such as elemental analysis, high resolution mass spectrometry (HRMS), infrared, ^{1}H, ^{13}C and COSY NMR, UV-visible absorption, thermogravimetric techniques have used to confirm the formation of products. Further, molecular structures of Ni(II)-dithiocarbamate macrocyclic complex **1** have been determined by single crystal X-ray diffraction (SCXRD) method. SCXRD analysis unveiled a monomeric centrosymmetric macrocyclic structure for complex **1** in which two bis-dithiocarbamate ligands are bridged over two Ni(II) metal ions through a S^S chelating mode resulting into a square planar geometry around each nickel centers. The geometries of all the M(II)-dithiocarbamate

macrocyclic complexes **1-6** have been optimized by a density functional theory calculation with B3LYP/LanL2DZ basis sets to corroborate the experimental results. Homobimetallic dithiocarbamate macrocyclic complexes **1-3** were further investigated for their potentials as a molecular probe in sensing/ binding of environmentally hazardous dyes such as Acid Orange (II), Bromocresol green, Bromophenol blue, Bromothymol blue, Crystal violet, Methylene blue by means of UV-visible and ^{1}H NMR tools. Interestingly, **1** showed selective sensing of Acid Orange (II) with considerable blue shifting of absorption bands whereas **2** and **3** sense Bromocresol green, selectively with significant red shifting of absorption bands. The stochiometric determination of **1** and Acid Orange II (G-1), monitored by the gradual shifting in one of aromatic ^{1}H signal (6.95 ppm) during titration study reveals the formation of 3:1 host-guest complex.

3.1 Introduction

Dyes used in textile industries often discharged in untreated effluents are considered to be serious threats to the environment and human health.[1] As estimated, approximately 7×10^{7} tons of synthetic dyes produced yearly through textile, dyeing, printing, tannery, paint, paper, pulp, cosmetics, leather, plastics, rubber and human health industries,[2] out of which 15–50% of the dyes entering into wastewater are discharged without a proper treatment. Based on their origin, structure, and usage, dyes are divided into several categories;[3] however, the anionic, azo, and sulfide dyes are widely used in textile coloring. Their untreated effluents usually contaminate both water (underground and surface water bodies) and soils. The mutagenic and carcinogenic nature, higher degree of stability, eradicating interaction to the ecosystem, and reduction of photosynthesis rate for the aquatic lives often result in severe environmental pollution.[4] In particular, 15–50% of largely used azo dyes that are not bound to fibers due to inefficient textile dyeing processes, releases into water bodies[5] and induces serious ecotoxicological threats as well as toxic effects on living organisms. For instance, azo dyes ingested by fish can be metabolized into toxic intermediates, creating the negative impact on fish and the health of their predators.[6] Moreover, farmers in developing countries irrigate their farming lands with polluted wastewater which ultimately give a negative impact on soil quality and crop germination rates.[5b, 7] On the other hand, the bromocresol green (BCG), an anionic and non-biodegradable dye is known to induce malignant cancer cells even at a small concentration i.e., <400 ppm.[8] Reports further suggests that approximately 47% of the world's population will face the challenge of clean water scarcity by the year 2030.[9] Therefore, the development

of efficient techniques for the removal of textile dyes is gaining utmost recognition around the world to achieve the goal of having safe and clean drinking water. Several methods including physical (adsorption, ion exchange, membrane filtration),[10] chemical (coagulation-flocculation, electrochemical, and advanced oxidation processes[11] and biological[12] or utilizing a combination of these methods have all been investigated for dye removal.

Inappropriately, the resources needed by most of the middle- and low-income countries for cleaning water are expensive, and therefore not feasible. As compared to the physical and chemical methods, the biological methods for wastewater remediation are more cost effective, environmentally friendly, and widely acceptable, but they are less effective and requires a long period of time to administered. The application of nanocatalysts[13] *viz.* Fe_3O_4/multiwalled carbon nanotubes,[13a] spinel-type $ZnAl_2O_4$,[13b] nano-ZnO/perlite,[13c] Fe–Ni bimetallic nanoparticles,[13d] Mn/Mg/Ce ternary ozone catalyst,[13e] Ag and Au nanoparticles decorated on chitosan-functionalized graphene oxide,[13f] $CoFe_2O_4$/ZnO nanocatalysts,[13g] AgCl nanocatalyst,[13h] and $CaFe_2O_4$ nanoparticles[13i] are reported to boost the degradation and mineralization of dyes. However, most of the known methods for dye removal suffers from additional challenges due to the toxic metabolites and by-products formed during the treatment process and high operational and maintenance costs.[11b, 14]

Reports further revealed that neutral organic macrocycles such as cyclodextrins and Calix[n]arenes *etc.*[15] have been shown to provide similar binding preferences and additional hydrogen bonding motifs for binding/ sensing of organic guests including a range of dyes. However a class of inorganic macrocyclic compounds[16, 17, 18] showing potential applicability in vitro-biological study, reversible thermochromism, neutral (1,4-dioxane, piperazine), anion ($H_2PO_4^-$, CH_3COO^-,$C_6H_5COO^-$)/ cation (Li^+, Na^+, K^+, Cs^+) receptors, ion-pair recognition, gas storage sensing, metal-sulphide nanoparticle synthesis *etc* but to the best of our knowledge, they have not been explored for either sensing or binding with organic dyes. Considering all the above facts, our aim was to develop dinuclear macrocyclic dithiocarbamate complexes holding *N*-bound organic thiophenylethyl and cyclohexyl moieties and to study the effect of electronic changes on their selective sensing/ binding ability with various hazardous dye stuffs.

In this chapter, A coordination driven self-assembling process involving diamines **H_2L^1** or **H_2L^2** with CS_2 and transition metal ion has led to new series of homobimetallic dithiocarbamate macrocyclic complexes [$M(II)_2$-μ^2-bis-{κ^2S^S-

$S_2CN(R)CH_2C_6H_3(OH)\}_2CH_2]$ (R = 2-thiophenylethyl; Ni(II) **1**, Cu(II) **2**, Zn(II) **3;** R = cyclohexyl; Ni(II) **4**, Cu(II) **5**, Zn(II) **6**).

The newly synthesized homobimetallic dithiocarbamate macrocyclic complexes were characterized spectroscopically, crystallographically and these were further investigated as potential small-molecule probes for sensing/ binding of hazardous dyes Acid Orange (II), bromocresol green, bromophenol blue, bromothymol blue, crystal violet and methylene blue by UV-visible absorption and ^{1}H titration study. In anticipation, the incorporation of the of transition metal ions as added features to show variable coordination and oxidation number, geometry, color, redox and electronic properties, these homobimetallic dithiocarbamate macrocyclic complexes would be established as better molecular probe in the detection and binding affinity towards hazardous waste water containing organic dyes.

3.2 Experimental Section

3.2.1 Materials and Instrumentations

All the synthetic operations were performed in an open atmosphere. Solvents were purchased from the commercial sources and were freshly distilled prior to use. Reagents were procured from Merck and Sigma-Aldrich Chemicals Limited; these were used without further purification. Ligand precursors 4,4'-methylenebis-2-((2-thiophen-2-yl)ethylamino)methylphenol (**H_2L^1**) and 4,4'-methylenebis-2-(cyclohexylmethylamino)methylphenol (**H_2L^2**) were synthesized following the literature procedure. The reaction and manipulations were performed at room temperature. Thin Layer Chromatography was performed on Merck 60 F254 aluminium-coated plates. Elemental analyses were performed on a Perkin-Elmer Series II CHNS Analyzer 2400. High resolution mass spectrometry (HRMS) analysis was performed by using an instrument Waters, Synapt XS HDMS containing a separation module of UPLC Acquity H class series system under electro spray positive (ES+) ionization mode. FTIR (KBr pellets) spectra of the samples were recorded in the 4000–400 cm^{-1} range using a Bruker FTIR spectrometer. The NMR experiments were carried out on a Bruker AV-III 400 MHz spectrometer in spectrometer with $CDCl_3$/DMSO-*d6* solvent and TMS as internal standard. UV-visible absorption were recorded on a JASCO V-730 UV-visible spectrophotometer. TGA/DTA plots were obtained using SII TG/DTA 6300 in flowing N_2 with a heating rate of 10 °C min^{-1}. The geometry of the molecules was optimized with the Gaussian 16 program and molecular orbitals were generated using GaussView 6.0 program.

3.2.2 Synthesis of homobimetallic dithiocarbamate macrocyclic complexes [M(II)$_2$-μ^2-bis-{κ^2*S*^*S*-$S_2CN(R)CH_2C_6H_3(OH)$}$_2CH_2$] (R = 2-thiophenylethyl; Ni(II) 1, Cu(II) 2, Zn(II) 3; R = cyclohexyl; Ni(II) 4, Cu(II) 5, Zn(II) 6)

To a 1 equivalent solution of diamine ligand precursors 4,4'-methylenebis-2-((2-thiophen-2-yl)ethylamino)methylphenol, **H_2L^1** (0.48 g, 1 mmol) and 4,4'-methylenebis-2-(cyclohexylmethylamino)methylphenol, **H_2L^2** (0.42 g, 1 mmol) in acetonitrile was added 2.1 equivalent of potassium hydroxide (0.12 g, 2.1 mmol) and the mixture was stirred for half an hour at room temperature and then excess of carbon disulfide (~10 mmol) was added and the reaction mixture was further stirred for 4 hours at room temperature. During this time, a change in color from colourless to pale yellow was noted. To this reaction mixture, $Ni^{II}(C_2H_3O_2)_2.4H_2O$ (0.25 g, 1 mmol), $Cu^{II}(C_2H_3O_2)_2.H_2O$ (0.20 g, 1 mmol) or $Zn^{II}(C_2H_3O_2)_2.2H_2O$ (0.22 g, 1 mmol) was added and the stirring was continued for 12 hours at room temperature. The residue was filtered and washed several times by water and then by n-hexane. The residue was dried under high vacuum to yield the corresponding products **1**-**6**. The compounds are taken for analysis and further study.

Table 1. Micro- and IR analysis data for complexes **1-6**.

Entry	Molecular Formula	Molecular Weight	Yield (%)	Melting/Dec. Point (°C)	Elemental Analysis % Found (calculated)				IR data (KBr disc) υ_{max}/cm^{-1}
					C	H	N	S	
1	$C_{58}H_{56}N_4O_4S_{12}Ni_2$	1375.22	85	198	50.74 (50.66)	4.17 (4.10)	4.15 (4.07)	28.03 (27.98)	3393(s), 2920(w), 2843(w), 1611(w), 1497(s), 1425(s), 1353(w), 1269(w), 1226(w), 1207(s), 1164(w), 1106(s), 1015(w), 962(w), 932(w), 823(w), 772(w), 697(s), 617(w), 577(w), 497(w)
2	$C_{58}H_{56}N_4O_4S_{12}Cu_2$	1384.92	64	172	50.38 (50.30)	4.16 (4.08)	4.12 (4.05)	27.83 (27.78)	3420(s), 2927(w), 1690(w), 1642(w), 1611(w), 1493(s), 1425(s), 1346(w), 1270(w), 1203(s), 1114(s), 1049(w), 979(w), 820(w), 769(w), 697(s), 617(s), 496(w)
3	$C_{58}H_{56}N_4O_4S_{12}Zn_2$	1388.59	89	160	50.22 (50.17)	4.13 (4.07)	4.08 (4.03)	27.76 (27.71)	3421(s), 2922(w), 1612(w), 1486(s), 1418(s), 1351(w), 1257(w), 1205(s), 1163(w), 1106(w), 1013(w), 962(w), 822(w), 771(w), 698(s), 577(w), 498(w)
4	$C_{58}H_{72}N_4O_4S_8Ni_2$	1263.10	85	230	55.21 (55.15)	5.80 (5.75)	4.51 (4.44)	20.39 (20.31)	3317(s), 2931(s), 2854(s), 1612(w), 1476(s), 1427(w), 1351(w), 1324(w), 1263(w), 1242(w), 1207(w), 1119(s), 1008(w), 969(w), 895(w), 817(w), 770(w), 671(w), 618(s), 573(w), 538(w), 493(w), 462(w)
5	$C_{58}H_{72}N_4O_4S_8Cu_2$	1272.81	74	196	54.81 (54.73)	5.75 (5.70)	4.44 (4.40)	20.22 (20.15)	3400(s), 2933(s), 2855(s), 1640(w), 1613(s), 1506(s), 1473(s), 1448(s), 1351(w), 1323(w), 1241(w), 1159(w), 1105(s), 1055(w), 1008(w), 896(w), 821(w), 772(s), 617(w)
6	$C_{58}H_{72}N_4O_4S_8Zn_2$	1276.48	87	210	54.64 (54.58)	5.73 (5.69)	4.45 (4.39)	20.17 (20.09)	3380(s), 2928(s), 2853(s), 1610(w),1563(w), 1502(w), 1449(s), 1416(s), 1350(w), 1322(w), 1241(s), 1205(w), 1160(s), 1101(s), 1008(s), 966(s), 895(w), 815(s), 767(w), 667(w), 613(w), 570(w), 542(w), 493(w), 468(w)

Table 2. NMR spectral data for complexes **1, 3, 4, 6**.

Entry	NMR Data (ppm)	
	^{1}H NMR	**^{13}C NMR**
1	6.66-7.28 (m, 24H, Ph and Th); 4.99 (s, 4H, Ph-C*H*$_2$-Ph); 3.82 (s, 8H, Ph-C*H*$_2$N); 3.12 (t, 8H, -C*H*$_2$NCS$_2$); 1.69 (t, 8H, -C*H*$_2$Th)	206.0 (-*N*^{13}*C*S$_2$), 154.6, 139.7, 132.9, 130.0, 127.6, 126.3, 126.1, 125.1, 120.6, 115.6, 51.4, 27.3
3	9.56 (broad s, 4H, -OH); 6.74-7.38 (m, 24 H, Ph/Th); 3.58 (s, 4H, Ph-CH$_2$-Ph); 3.43 (s, 8H, Ph-C*H*$_2$N); 3.28 (t, 8H, -C*H*$_2$NCS$_2$); 1.86 (t, 8H, -C*H*$_2$Th)	207.35(-*N*^{13}*C*S$_2$), 153.55, 141.00, 133.22, 128.91, 128.31, 127.59, 125.92, 124.36, 123.16, 115.58, 55.55, 52.63, 27.05, 23.91
4	9.630 (broad s, 4H, -OH); 6.44-7.09 (m, 12H, Ph); 4.67 (s, 4H, Ph-C*H*$_2$-Ph); 3.75 (merged s, 8H, -C*H*$_2$NCS$_2$); 0.951-1.718 (m, 44H, Cy)	208.1 (-*N*^{13}*C*S$_2$), 152.9, 138.8, 138.5, 133.7, 129.3, 128.6, 127.7, 127.4, 127.2, 122.5, 115.7, 115.5, 57.4, 44.2, 17.1, 16.4, 14.8
6	9.42 (broad s, 4H, -O*H*); 6.67-7.05 (m, 12H, Ph); 4.94 (s, 4H, Ph-C*H*$_2$-Ph); 3.39 (s, 8H, -C*H*$_2$NCS$_2$); 1.05-1.84 (m, 44H, Cy)	205.9 (-*N*^{13}*C*S$_2$), 152.2, 132.3, 127.8, 126.1, 123.1, 115.1, 63.9, 47.6, 30.3, 25.7, 25.2

3.3 Result and Discussion

3.3.1 Synthesis and Characterization

Secondary diamines viz. 4,4'-methylenebis-2-((2-thiophen-2-yl)ethylamino)methylphenol (**H_2L^1**) and 4,4'-methylenebis-2-(cyclohexylamino)methylphenol (**H_2L^2**) have been synthesized in chapter 2. Further derivatization of diamines **H_2L^1** and **H_2L^2** into homobimetallic dithiocarbamate macrocyclic complexes [M(II)$_2$-μ^2-bis-{κ^2*S*^*S*-$S_2CN(R)CH_2C_6H_3(OH)\}_2CH_2$] (R = 2-thiophenylethyl; Ni(II) **1**, Cu(II) **2**, Zn(II) **3**; R = cyclohexyl; Ni(II) **4**, Cu(II) **5**, Zn(II) **6**) have been performed by using a single pot reaction involving diamine **H_2L^1** or **H_2L^2** with CS_2 and transition metal Ni(II), Cu(II) or Zn(II) ion as per Scheme 1 which has shortens the workup and ultimately save valued resources.

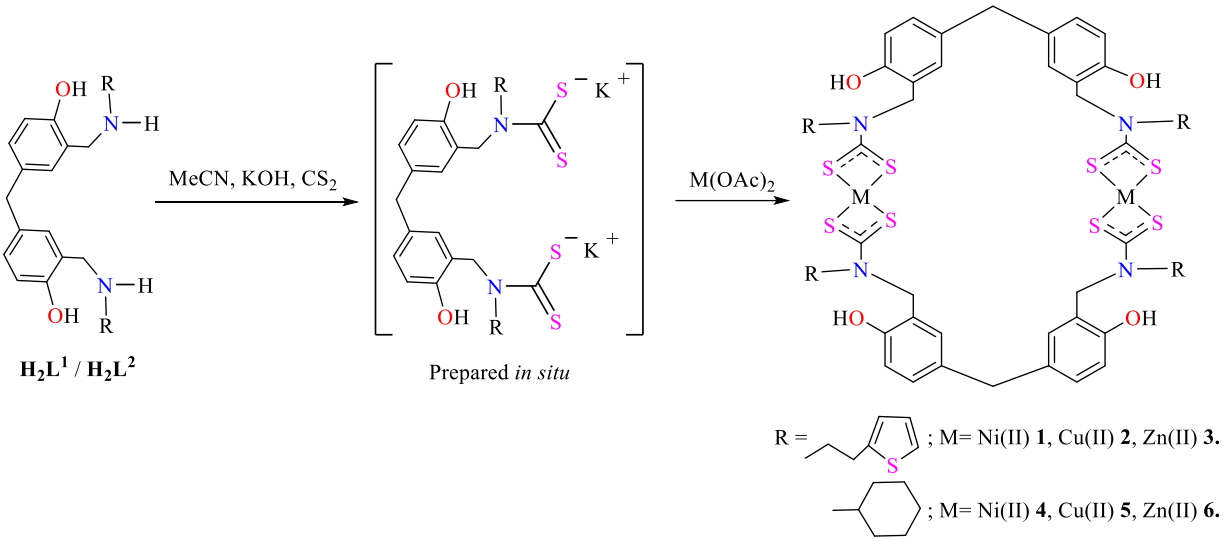

Scheme 1. Synthesis of new homobimetallic dithiocarbamate macrocyclic complexes bearing functionalized linker framework.

The green solid Ni(II)-dithiocarbamate (**1** and **4**), brown solid Cu(II)-dithiocarbamate (**2** and **5**) and pale yellow solid Zn(II)-dithiocarbamate (**3** and **6**) compounds showed good solubility in a solvent like DMSO/ DMF and these are found to persist in the solid state and in the solution over a period of days.

The formulation and purity of all the compounds were confirmed by microanalysis, relevant spectroscopic (HRMS, ^{1}H, ^{13}C, COSY NMR, IR, UV-visible), thermogravimetric and crystallographic studies, corroborated by DFT level calculations. The microanalysis data obtained for all the compounds are in good agreement with their compositions and mutually supported by subsequent spectroscopic and theoretical studies. The analysis data for

homobimetallic dithiocarbamate macrocyclic complexes **1-6** is tabulated in table 1 and table 2.

The mass analysis was carried out by electrospray ionization (ESI) mode with set parameters, such as gas temperature: 250 °C; drying gas flow: 12 $Lmin^{-1}$; nebulizer pressure: 35 psig; sheath gas flow: 11 $Lmin^{-1}$, sheath gas temperature: 300 °C. The scan source parameters were maintained at capillary voltage: 3.5KV; nozzle voltage: 1.0KV, fragmentor voltage: 175 V; skimmer voltage: 65 V. Mass spectrometric data was processed using MassHunter™ B.08.00 software. HRMS spectra of these compounds gave high resolution mass peak for **2** ($C_{58}H_{56}N_4O_4S_{12}Cu_2$) 1383.8928 $[M-H]^+$ and **3** ($C_{58}H_{56}N_4O_4S_{12}Zn_2$) 1388.8915 $[M+H]^+$.

All the compounds displayed characteristic IR bands due to ν(O-H), ν(C-H), ν(C=C), ν(C-N), ν(C-C) and ν(CS_2) groups in the expected IR regions in their corresponding IR spectrum. The disappearance of ν(N-H) band of free diamines **H_2L^1/ H_2L^2** at ~3260 cm^{-1} (chapter 2) and advent of new single sharp medium intensity bands in 979-896 cm^{-1} and 498-462 cm^{-1} ranges due to $\nu_{assy}(CS_2)$ and ν(Ni-S) in the IR spectra of homobimetallic dithiocarbamate macrocyclic derivatives **1-6** validates bidentate coordination of dithiocarbamate ligands.[18a, 19] Besides, compounds holding peripheral thiophene substituents gave a medium intensity band in 822-722 cm^{-1} range, attributable to C–S–C out-of-plane deformation whereas a strong band appeared in 698-618 cm^{-1} range, is assignable to the out-of-plane deformation of the C–H group, a characteristic of substituted thiophene.[20] An appreciable augmentation in the ν(C–N) frequency of **1-6** in comparison to similar frequency observed in unbound diamine precursors **H_2L^1-H_2L^2**, specifies the status of electron delocalization over coordinated dithiocarbamates (R = N^+–CS_2^-). The IR data is well supported by corresponding NMR spectral study. The various methylene protons and aromatic protons have appeared in the expected range in the ^1H NMR spectrum of all the compounds. The assignment of ^1H NMR spectral data is well supported by ^{13}C and 2D NMR study. Notably, the signals of CH_2Th and N-CH_2 protons along with CH_2Ph experiences significant deshielding effects in their dithiocarbamate complexes **1-6**. The formation of discrete homobimetallic dithiocarbamate macrocyclic structures is ascertained by the appearance of sharp signals with resolved splitting patters, except a few multiple sets of overlapped peaks in the NMR spectra of **1-6**. The ^{13}C NMR spectra of homobimetallic dithiocarbamate macrocyclic complexes gave most characteric singals in 205.9-208.1 ppm range and confirms the poresence of coordinated dithiocarbamate (-N$^{13}CS_2$) moieties.[18, 19]

3.3.2 UV-Visible absorption spectral study

The electronic absorption spectrum homobimetallic dithiocarbamate complexes **1-6** was recorded in 10^{-5} M DMF solution at room temperature (Figure 1, Table 3) All the homobimetallic complexes **1-6** display three prime absorption bands in 275-284 nm, 315-335 nm and 395-442 nm regions, due to intramolecular π→π*, n→π* and charge transfer transitions, respectively, apart from a d-d band in 629-643 nm regions, except Zn(II)-dithiocarbamate macrocycles **3** and **6**. The nature of absorption bands along with magnetic moment values (Table 3) further indicate the presence of square planar / distorted square planar Ni(II)/ Cu(II) and distorted tetrahedral Zn(II) ions in M(II)-dithiocarbamate macrocycles **1-6**.[18]

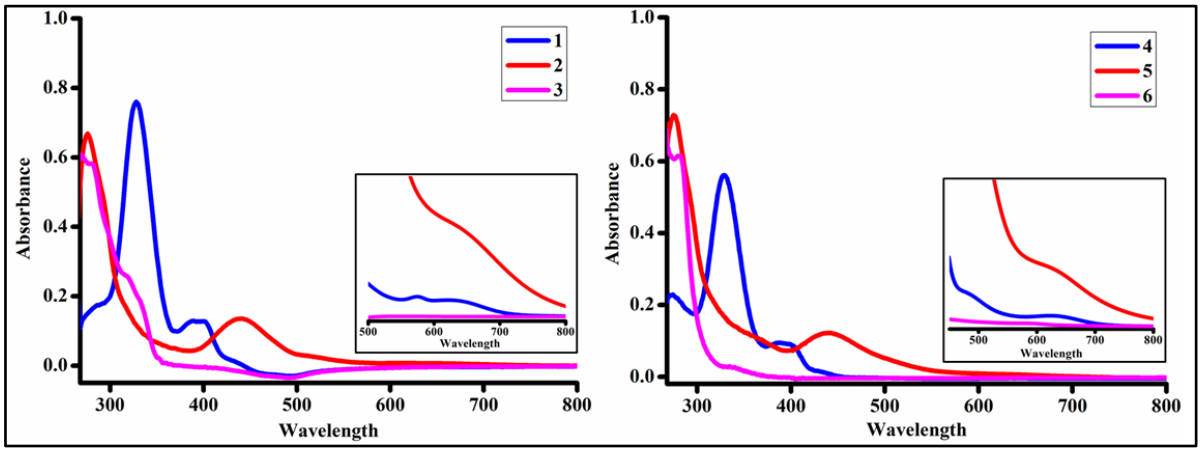

Figure 1. UV-visible absorption spectra of homobimetallic macrocyclic dithiocarbamate complexes **1-6** in 10^{-5} M DMF solution at room temperature.

Table 3. UV-visible absorption data for homobimetallic macrocyclic dithiocarbamate complexes **1-6** recorded in 10^{-5} M DMF solution.

Entry	UV-Visible data (10^{-5} M DMF) λ_{max} nm (ε, L mol^{-1} cm^{-1})	Magnetic moment μ_{eff} (BM)
1	280 (16964) π→π*, 326 (76066) n→π*, 395 (13215) CT, 629 (201) d-d	0
2	275 (67095) π→π*, 315 (17086) n→π*, 440 (13722) CT, 643 (940) d-d	1.88
3	279 (58509) π→π*, 318 (26096) n→π*, 400 (193) CT	0
4	271 (22113) π→π*, 328 (56258) n→π*, 392 (9397) CT, 630 (174) d-d	0
5	275 (73025) π→π*, 321 (19639) n→π*, 442 (12259) CT, 626 (807) d-d	1.92
6	280 (61659) π→π*, 335 (2903) n→π*, 370 (163) CT	0

3.3.3 Thermogravimetric Analysis

The thermogravimetric study on homobimetallic dithiocarbamate macrocyclic derivatives **1-6** was performed in the temperature ranges from room temperature to 750 ºC to understand thermal stability and degradation patterns. The heating rate was suitably controlled at 10 ºC min^{-1} under N_2 atmosphere. The temperature ranges recorded on TGA curves agreeing to percentage weight loss on TG curves during the degradation and stable residual mass obtained are summarized in the table 4. A multistage mass loss on DTG curves due to endothermic and/or exothermic elimination of molecular fragments can be clearly visualized by thermogravimetric plots (Figure 2). Notably, the thermal degradation of **1-6** start before their melting points and the thermal stability of homobimetallic dithiocarbamate macrocyclic complexes **1-3** found to be superior than other complexes **4-6** which gave a stable residual mass, attributable to corresponding MSO_4 (Table 4).

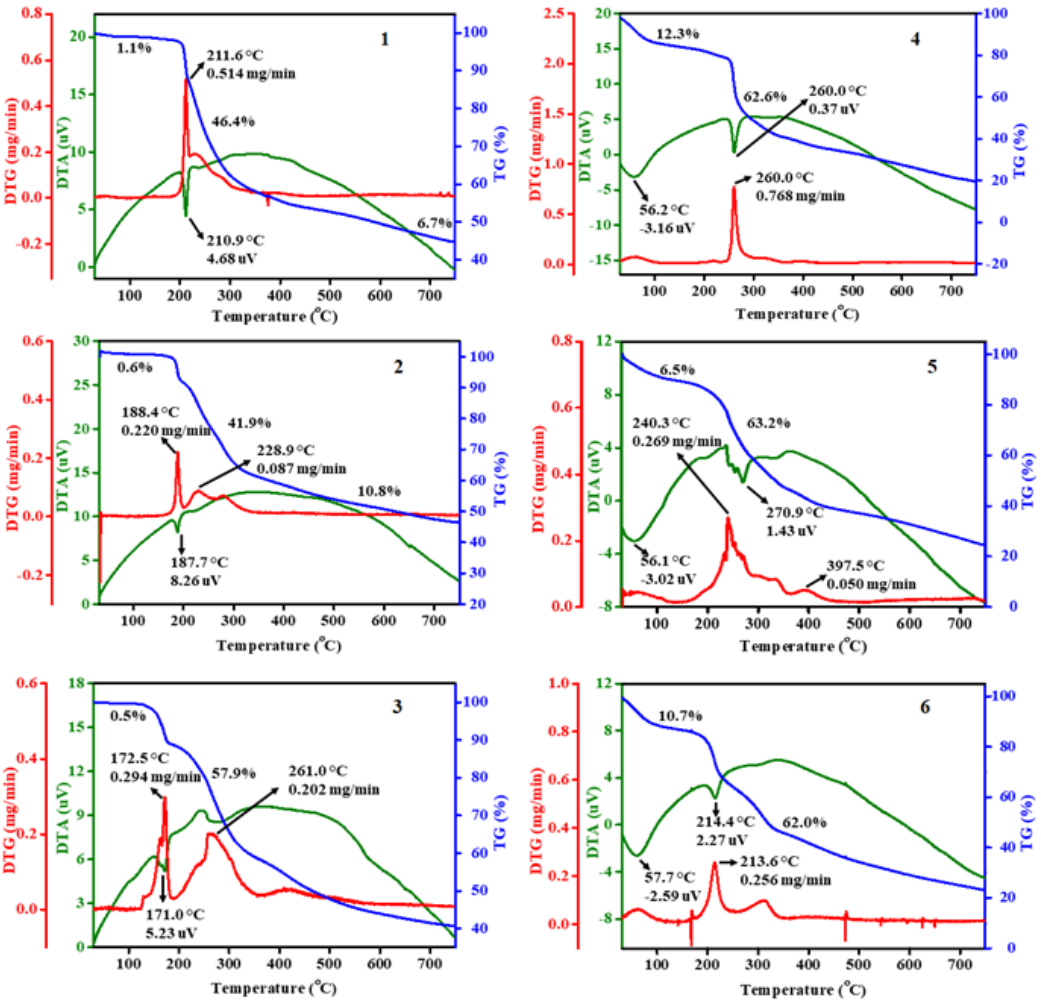

Figure 2. TG/DTA curves for homobimetallic macrocyclic dithiocarbamate complexes **1-6**.

Table 4. Thermogravimetric analysis of homobimetallic macrocyclic dithiocarbamate complexes **1-6.**

Entry	T (°C) in DTA	T (°C) in TGA	Mass loss obs. (%) in TG	Residue wt. obs. (Calcd.) (%)	Expected product of decomposition
1	210.9	180-400	46.4	46.9	Mass loss continues
		400740	6.7		
2	187.7	185-400	41.9	47.3	Mass loss continues
		400-740	10.8		
3	171.0	150-740	57.9	42.1	Mass loss continues
4	56.2	50-200	12.3	25.1	$NiSO_4$
	260.0	200-740	62.6	(24.5)	
5	56.1	60-200	6.5	30.3	$CuSO_4$ + char
	270.9	200-740	63.2	(25.1)	
6	57.7	50-150	10.7	27.3	$ZnSO_4$
	214.4	150-740	62.0	(25.3)	

3.3.4 X-ray crystallographic study

The single crystal of homobimetallic dithiocarbamate macrocyclic complex **1** suitable for single crystal X-ray diffraction (SCXRD) study was grown by slow evaporation from dimethylformamide solutions. Molecule of 1.*2DMF* crystallize in the triclinic P-1 space group. The crystal structure of **1** show asymmetric unit cell of 1.*2DMF* displays half of the molecule and its complete molecule is generated through symmetry operation are shown in Figure 3. The crystallographic data and structure parameters for 1.*2DMF* are given in Table 5.

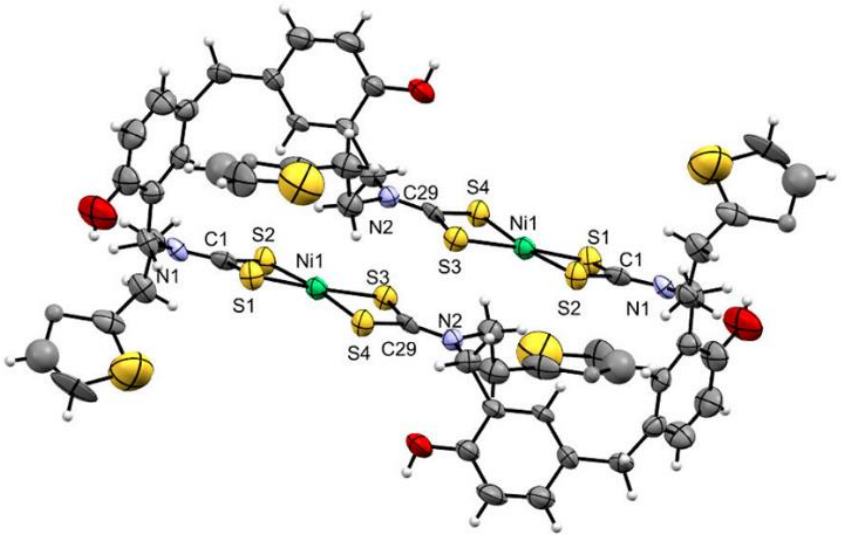

Figure 3. *ORTEP* diagram with partial atoms labelled showing 40% probability ellipsoids for 1.*2DMF*.

Table 5. Crystal data and structure refinement for homobimetallic dithiocarbamate macrocyclic complex **1.**

Identification Code	**1.*2DMF***
CCDC Number	2248633
Formula	$C_{36}H_{36}N_4NiO_4S_6$
Formula weight	839.76
Temperature/K	293
Crystal system	triclinic
Space group	P-1
a/Å	9.8418(10)
b/Å	14.3020(12)
c/Å	15.2073(16)
α/°	97.433(8)
β/°	108.028(9)
γ/°	97.839(8)
Cell volume/Å^3	1982.7(4)
Z	2
ρ_{calc}g/cm^3	1.407
μ/mm^{-1}	0.848
F(000)	872.0
Radiation	Mo Kα (λ = 0.71073)
2Θ range for data collection/°	5.964 to 58.452
	-13 ≤ h ≤ 12, -19 ≤ k ≤ 19, -20 ≤ l ≤ 20
Reflections collected	42919
Independent reflections	9612 [R_{int} = 0.2040, R_{sigma} = 0.2341]
Data/restraints/parameters	9612/0/439
Goodness-of-fit on F^2	1.027
Final R indexes [I>=2σ (I)]	R_1 = 0.1277, wR_2 = 0.2466
R indexes [all data]	R_1 = 0.2750, wR_2 = 0.3201
Larg. diff. peak/hole /eÅ^{-3}	1.10/-0.61
Flack parameter	-0.02(2)

In the homobimetallic dithiocarbamate macrocyclic complex **1**, significant decrease in the ∠ Ph-CH_2-Ph (114.64°) and increase in the ∠ Ph-CH_2-N (112.55-113.83°) and ∠ CH_2-N-CH_2 (118.31-116.82°), compared to similar bond angles observed in its diamine ligand precursor **H_2L^1** (∠ Ph-CH_2-Ph = 117.03°, ∠ Ph-CH_2-N = 111.02° and ∠ CH_2-N-CH_2 = 112.12°). Further, the dihedral angle between the least squares planes through the internal phenyl rings is 71.57º in diamine ligand precursor **H_2L^1** which is significantly larger than the similar angle observed in its complex **1**. Such flexibility associated with the linker framework is crucial for the formation of such inorganic macrocyclic compounds. Each Ni(II) centers in

complex **1** are bonded to soft sulphur-donor sites of bis-dithiocarbamate derivative of $\mathbf{H_2L^1}$ (prepared *in-situ*). The calculated dihedral angle between the least squares planes drawn through the chelate rings S1C1S2Ni1 and S3C29SS4Ni1 is 8.56º. The distortion in the geometry around Ni(II) centers from a regular square planar geometry can be clearly visualized (Figure 4) by the deviation in chelate ring planes from coplanarity and S−M−S angles from 90°.

It is noteworthy that a substantial decrease in the C-N (1.319-1.320 Å) bond distances of homobimetallic dithiocarbamate macrocyclic complex **1** is observed in comparision to the C-N (1.462 Å) bond distance of diamine ligand precursor $\mathbf{H_2L^1}$, The C-N, C-S and Ni–S bond distances of **1** is found to be comparable to similar distances observed in analogous square planar Ni(II) complex reported earlier.[21] A considerable decrease in the C-N bond distances of **1** while moving from free diamine $\mathbf{H_2L^1}$ to its dithiocarbamate derivative **1** indicate the rehybridization of nitrogen atoms ($sp^2 \rightarrow sp^2$) due to π-electron delocalization between the nitrogen and sulphur, which is corroborated by density functional theory calculations, later.

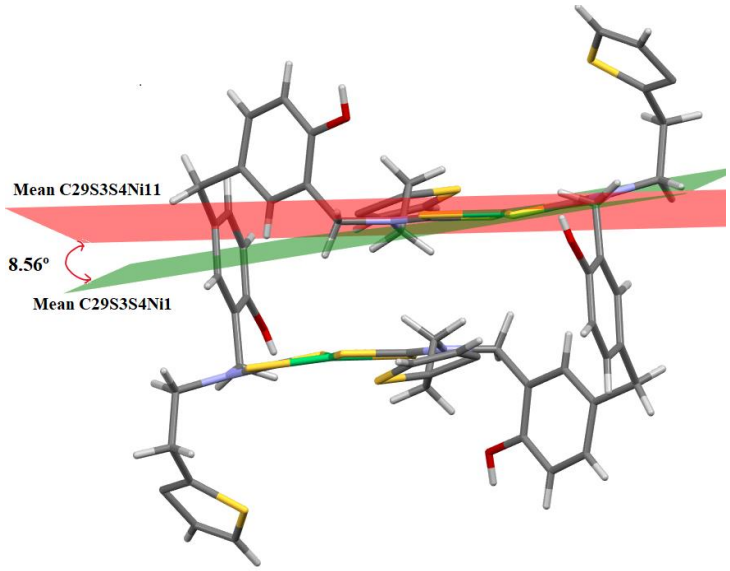

Figure 4. Deviation of geometry around Ni(II) centers from a regular square planar geometry (dihedral angle between the planes drawn through the mean of chelate rings S1C1S2Ni1 and S3C29SS4Ni1 = 8.56º).

Further, single-crystal data is valuable in figure out the supramolecular structures of $\mathbf{H_2L^1}$ and **1** also in evaluating the crucial role of various functionalities including solvent molecules present in the crystal structure on the association of molecules in the solid state. A careful assessment of the crystal data of $\mathbf{H_2L^1}$ and **1** revealed that the presence of several groups and solvent molecules makes electronic and structural variations that seemingly modify the nature and amount of donor-acceptor locations for inter- and intramolecular non-

covalent contacts such as OH…N, N-H…O, CH…S, C-H…O *etc.* contacts that led to diverse crystal packing shapes.

In the homobimetallic dithiocarbamate macrocyclic complex **1**, the electronic and structural parameters are changed (Figure 5a) in such a way that each molecules of **1** offer C3-H3B….S4 two closing contacts with neighbouring molecules, arranging the molecules linearly along *a*-axis, forming a comb like 1D molecular structure as shown by a spacefill model (Figure 5b).

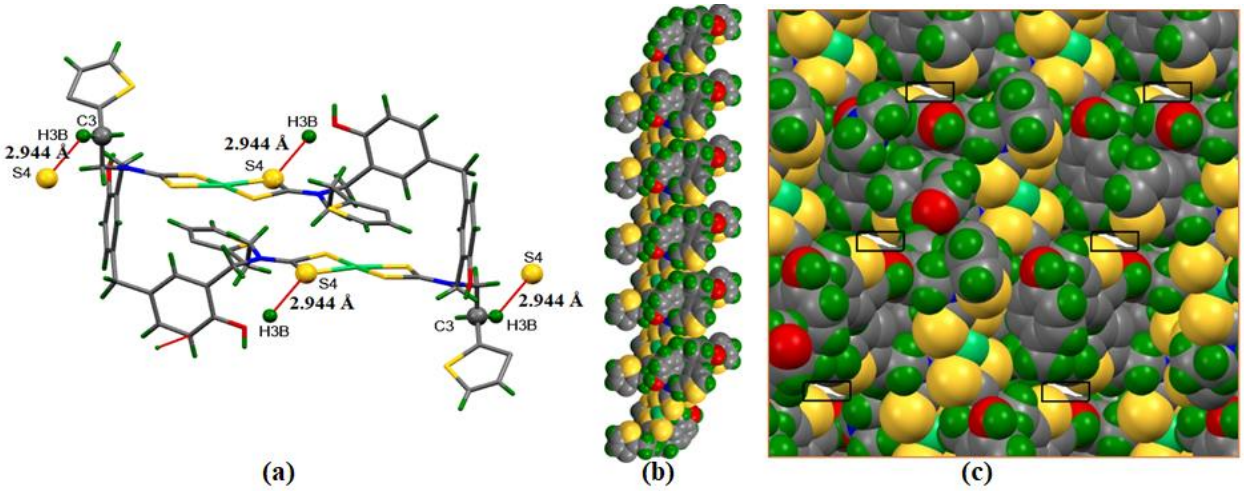

Figure 5. Asymmetric molecule of H_2L^1 displaying (a) opening of CH….S short-contact; (b) formation of comb like 1D molecular structure through CH…S intermolecular contacts; (c) spacefill model presenting an attractive 3D multiple open tubular supramolecular assembly sustained by a vast number intermolecular contacts.

Further, the dimensionality of the supramolecular assembly formed sustained through C3-H3B….S4 intermolecular contacts is evidently extended three dimensionally by using a vast number of short contacts involving DMF solvent molecules, resulting into a fascinating 3D multiple opening of dimension: ~ 8.890 × 35.213 $Å^2$ as shown by a spacefill model (Figure 5c). This opens a scope for macrocyclic complex **1** and its analogues to be investigated as a potential host in the host-guest supramolecular chemistry and as a potential gas absorber for small sized molecules like H_2, N_2, CO_2 that needs validation to enrich the area of material Science.

3.3.5 Density functional theory calculations

To gain a better understanding of the experimental results and the properties of homobimetallic dithiocarbamate macrocyclic complexes **1-6**, density functional theory

calculation has been accomplished by using at B3LYP/LanL2DZ basis set. All the geometry optimizations were performed with the Gaussian 16 program[22] and molecular orbitals were generated using GaussView 6.0 program.[23] Similar calculations were used in recent years due to its capability to accurately reproduce the structural features and properties of the large dithiocarbamates macrocyclic complexes obtained from single-crystal X-ray diffraction study.[24] The structures optimized for the minimum energy conformation of **1-6** and their molecular electrostatic potential (MESP) maps are provided in Figure 6 and Figure 7, respectively. The frontier molecular orbitals analysis (Figure 8), structural parameters (Table 6) and a brief summary of DFT study (Table 7) are summarized.

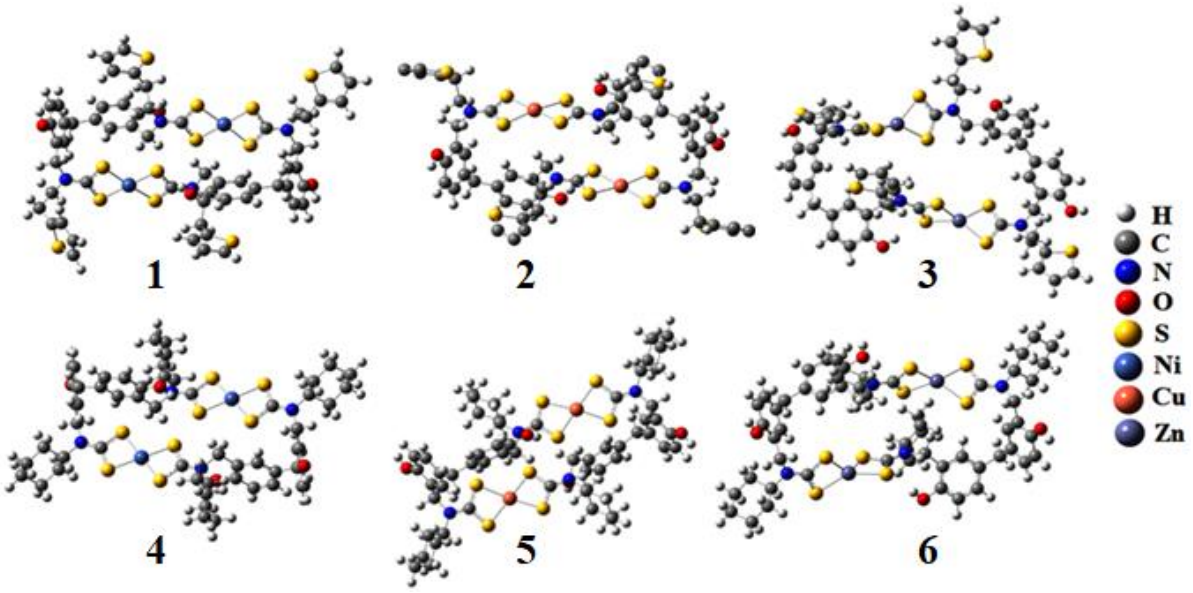

Figure 6. Perspective views of the lowest-energy optimized-geometry of homobimetallic dithiocarbamate macrocyclic complexes 1-6 at B3LYP/LanL2DZ.

A careful comparision of experimenatlly determined selected bond lengths (Å) and bond angles (º) of $\mathbf{H_2L^1}$ and its homobimetallic Ni(II)-dithiocarbamate macrocyclic complex **1** with theoretically obtained similar parametrs is tabulated in Table 6. The calculated structural parametrs are in good agreement with the similar values obtained from single crystal X-ray analysis and corroborates the theoretical calculations. Contrary to Cu–S bond distances (2.389-2.403 Å) of Cu(II)-dithiocarbamate macrocycles **2** and **5**, Ni–S bond distances (2.273-2.281 Å) of homobimetallic Ni(II)-dithiocarbamate macrocycles **1** and **4** (Table 6) are almost identical and indicates symmetrical isobidentate coordination mode of the dithiocarbamate moieties. Moreover, theoretically determined dihedral angle between the planes drawn through the mean of chelate rings (5.89°) of **1** is close to the experimentally determined similar angle 8.56º (Figure 4) and reinforce slight deviation of regular square

planar geometry around Ni(II) centers in **1** and **4** (*vide supra*). A critical analysis of theoretical data suggest distorted distortion of geometry around both the Zn(II) centers in **3** and **6** from tetrahedron. Similar to the experimental observation, the calculated structures of homobimetallic M(II)-dithiocarbamate macrocycles **1-6** provides C–N bond distances in 1.319–1.345 Å range which suggests the presence of sp^2 hybridized nitrogen atoms due to π-electron delocalization between the nitrogen and sulphur of coordinated dithiocarbamate moities.

Mapping of molecular electrostatic potentials (MESP) designates the area of low and high electron density in the molecular framework. Red and blue colouring in the MESP images of complexes **1-6** (Figure 7) symbolizes localization of negative and positive potential, respectively. The localization of high electron density around dithiocarbamate moieties and low electron density around O-H of peripheral phenyl groups in **1-6**, indicates crucial sites available to offer a number of intermolecular H-bonding interactions (verified SCXRD study) and their ability to interact with inorganic, organic guest species. Moreover, the examination of highest occupied molecular orbitals (HOMO) and lowest occupied molecular orbitals (LUMO) of **1-6** revealed delocalisation of electrons over one of the dithiocarbamate chelate groups (in case of HOMO-LUMO **1**, **4** and **5**; HOMO of **2** and LUMO of **6**) and over one of the peripheral thriophenyl/cyclohexyl group (in case of HOMO-LUMO of **3**, LUMO of **2** and HOMO of **6**) as shown in Figure 8.

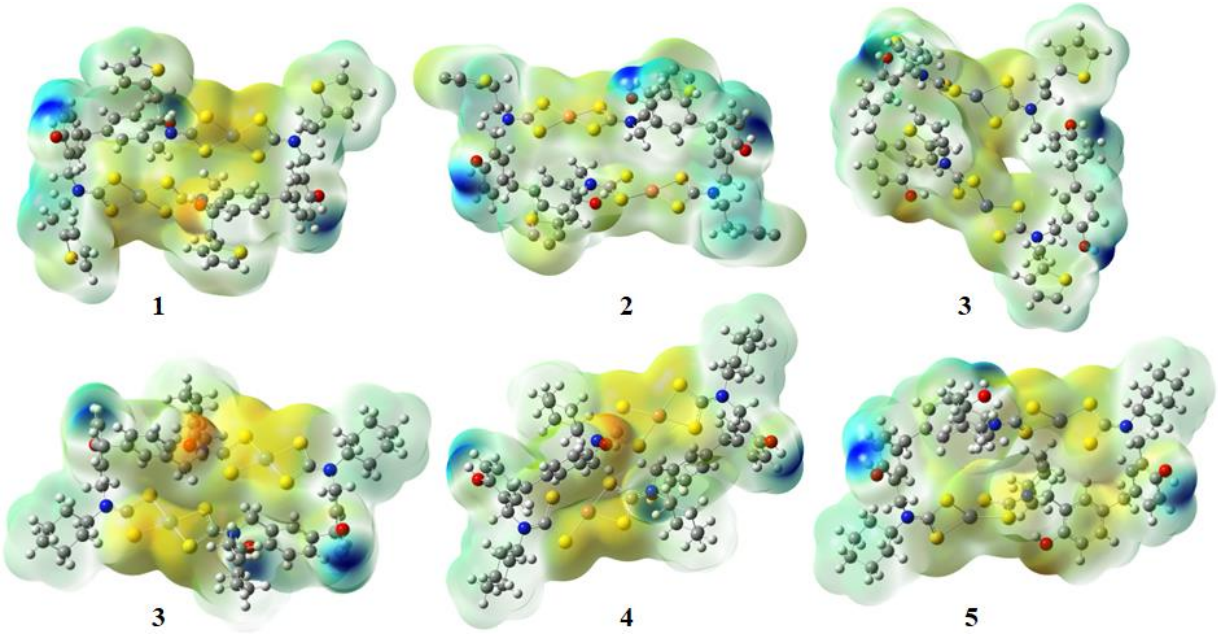

Figure 7. Molecular electrostatic potential (MESP) maps of homobimetallic dithiocarbamate macrocyclic complexes **1-6**.

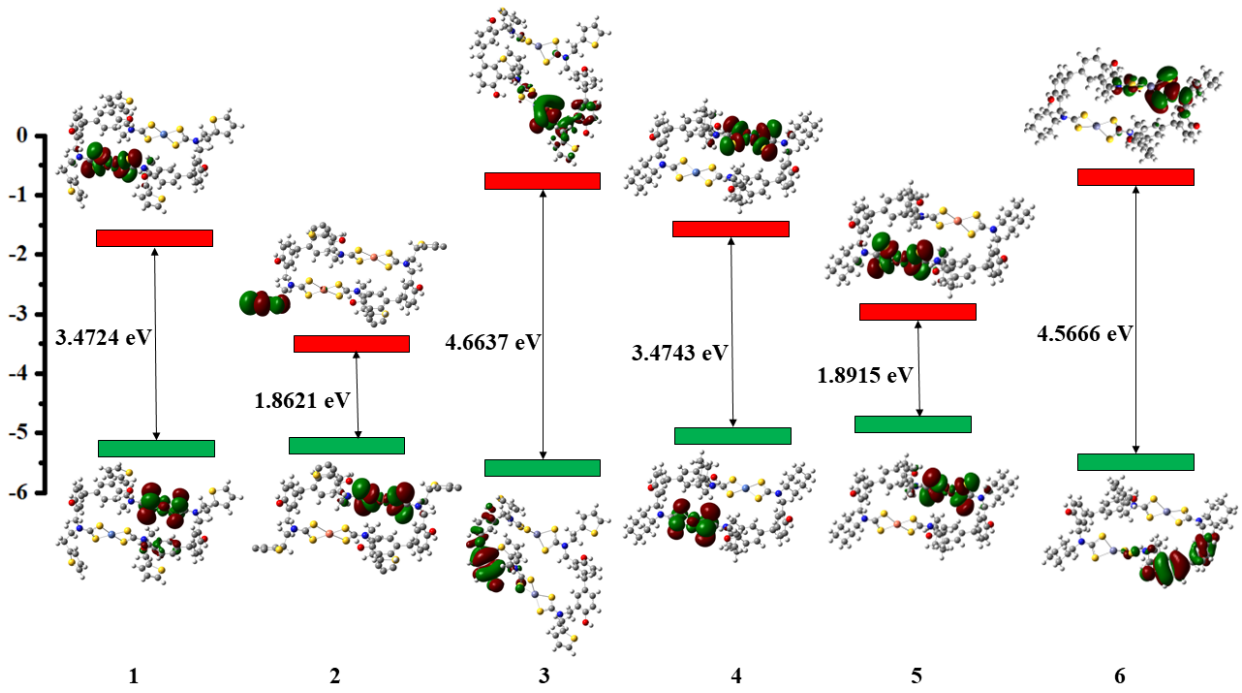

Figure 8. Frontier molecular orbitals derived from DFT calculations at B3LYP/6-31 (d,p) level for homobimetallic macrocyclic dithiocarbamate complexes **1-6**.

Table 6. Comparision of experimetal bond lengths (Å) and bond angles (º) with theoretical value obtained by DFT calculations.

Experimental data obtained from SCXRD (This work)				
1	Ni1-S1	2.197(3)	S1-Ni1-S2	79.02(9)
	Ni1-S2	2.221(2)	S1-Ni1-S3	175.52(10)
	C1-N1	1.319(11)	S1-C1-S2	110.20(5)
	C1-S1	1.702(8)	N1-C1-S1	125.40(7)
	C1-S2	1.724(9)	C14-C15-C16	114.7(7)
Theoretical data obtained from DFT (This work)				
1	Ni-S1	2.273	S1-Ni-S4	78.36
	Ni-S4	2.279	S1-Ni-S42	175.03
	C12-N9	1.343	S1-C12-S4	112.39
	C12-S1	1.731	N9-C12-S1	122.92
	C12-S4	1.729	C19-C30-C20	115.93
2	Cu-S1	2.389	S1-Cu-S4	75.51
	Cu-S4	2.403	S1-Cu-S63	171.43
	C13-N10	1.343	S1-C13-S4	115.53
	C13-S1	1.733	N10-C13-S1	122.04
	C13-S4	1.736	C20-C41-C24	115.41
3	Zn-S41	2.440	S41-Zn-S40	75.97
	Zn-S40	2.439	S41-Zn-S37	124.54
	C44-N45	1.341	S41-C44-S40	118.22
	C44-S41	1.749	N45-C44-S41	121.37
	C44-S40	1.751	C4-C10-C13	116.00
4	Ni-S1	2.275	S1-Ni-S4	78.27
	Ni-S4	2.281	S1-Ni-S42	174.60
	C12-N9	1.342	S1-C12-S4	112.08

	C12-S1 C12-S4	1.733 1.734	N9-C12-S1 C19-C30-C20	123.27 115.99
5	Cu-S1 Cu-S4 C12-N9 C12-S1 C12-S4	2.392 2.400 1.344 1.736 1.739	S1-Cu-S4 S1-Cu-S42 S1-C12-S4 N9-C12-S1 C19-C30-C20	75.35 168.97 114.90 121.83 115.61
6	Zn-S41 Zn-S40 C44-N45 C44-S41 C44-S40	2.454 2.441 1.345 1.747 1.752	S41-Zn-S40 S41-Zn-S37 S41-C44-S40 N45-C44-S41 C4-C10-C13	75.60 119.46 118.10 120.60 113.88

Further, calculated HOMO-LUMO gaps falls in the range of 1.86-1.89 eV (Table 7) for both the homobimetallic Cu(II)-dithiocarbamate macrocycles **2** and **5**, representing their semiconducting nature.[25]

Table 7. Summary of Computational study performed on complexes **1-6.**

Entry	Energy (Hartree)	HOMO (eV)	LUMO (eV)	Band Gap (eV)
1	-7880.774430	-5.4147	-1.9423	3.4724
2	-7926.236513	-5.4480	-3.5859	1.8621
3	-7673.354164	-5.6463	-0.9826	4.6637
4	-6297.774069	-5.2594	-1.7851	3.4743
5	-6351.428243	-4.9446	-3.0531	1.8915
6	-6090.335668	-5.5092	-0.9426	4.5666

3.4 Host-Guest Binding Study

The homobimetallic dithiocarbamate macrocyclic complexes **1-6** holding Lewis acidic transition metal ions and functionalized linkers were expected to be established as capable molecular probe to sense/ bind a range of hazardous organic dyes. The widespread pollution of natural water resources by hazardous organic pollutants has become an issue for many countries in recent years because of lack of specific and economically viable technique for providing an effective solution to such a problem.[25] Earlier, inclusion reactions of organic cyclodextrins with Acid Orange (II), monitored by stopped-flow method and UV-spectra[26] suggest that the naphthalene side is partially inserted into the cavity forming 1:1 host/guest complex. Recently, Professor Stoikov and his co-workers[27] have reported macrocycles pillar[5]arenes to selectively recognize methyl Orange by electrostatic, hydrophobic and π–π stacking interactions. Development of new cost effective probes that is rapid, facile and applicable to the environmental settings is an important goal of sensing community due to current concern over hazardous dyes and its toxic effects on human health.

This has inspired us to explore the potentials of selected homobimetallic dithiocarbamate macrocyclic complexes **1-3** as an effective host in binding with a range of dyes such as Acid Orange (II), bromocresol green, bromophenol blue, bromothymol blue, crystal violet and methylene blue (Figure 9) by using UV-visible and ^{1}H NMR titration study.

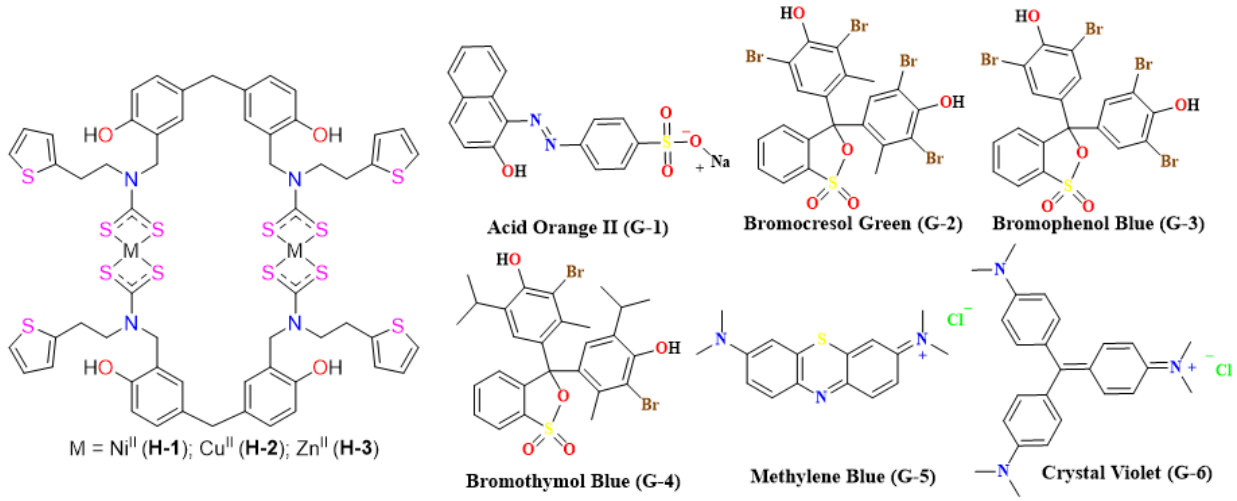

Figure 9. List of hosts and guests under investigation.

Evidently, a substantial increase in the intensity of absorption band occurs during the interaction of Acid Orange (II) and Ni(II)-dithiocarbamate macrocycles **1** with a concomitant blue shift of ≈ 6 nm as shown in Figure 10 (a). Contrarily, Cu(II)- and Zn(II)-dithiocarbamate macrocycles (**2** and **3**) showed selectivity towards Bromocresol Green as evidenced by a significant increase in the absorption band intensity of Bromocresol Green host-guest interaction with a concomitant red shift of ≈ 5-9 nm.

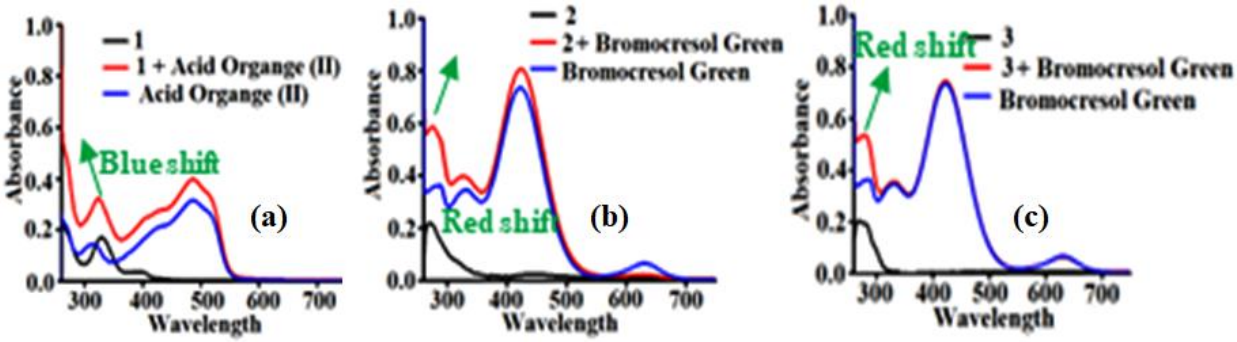

Figure 10. Sensing ability were examined by UV-visible spectroscopy displaying (a) a net blue shift of ≈6 nm of Ni(II) complex in presence of Acid Orange (II) dye. (b) a net red shift of ≈5 nm of Cu(II) complex in presence of Bromocresol green dye. (c) a net red shift of ≈9 nm of Zn(II) complex in presence of Bromocresol green dye.

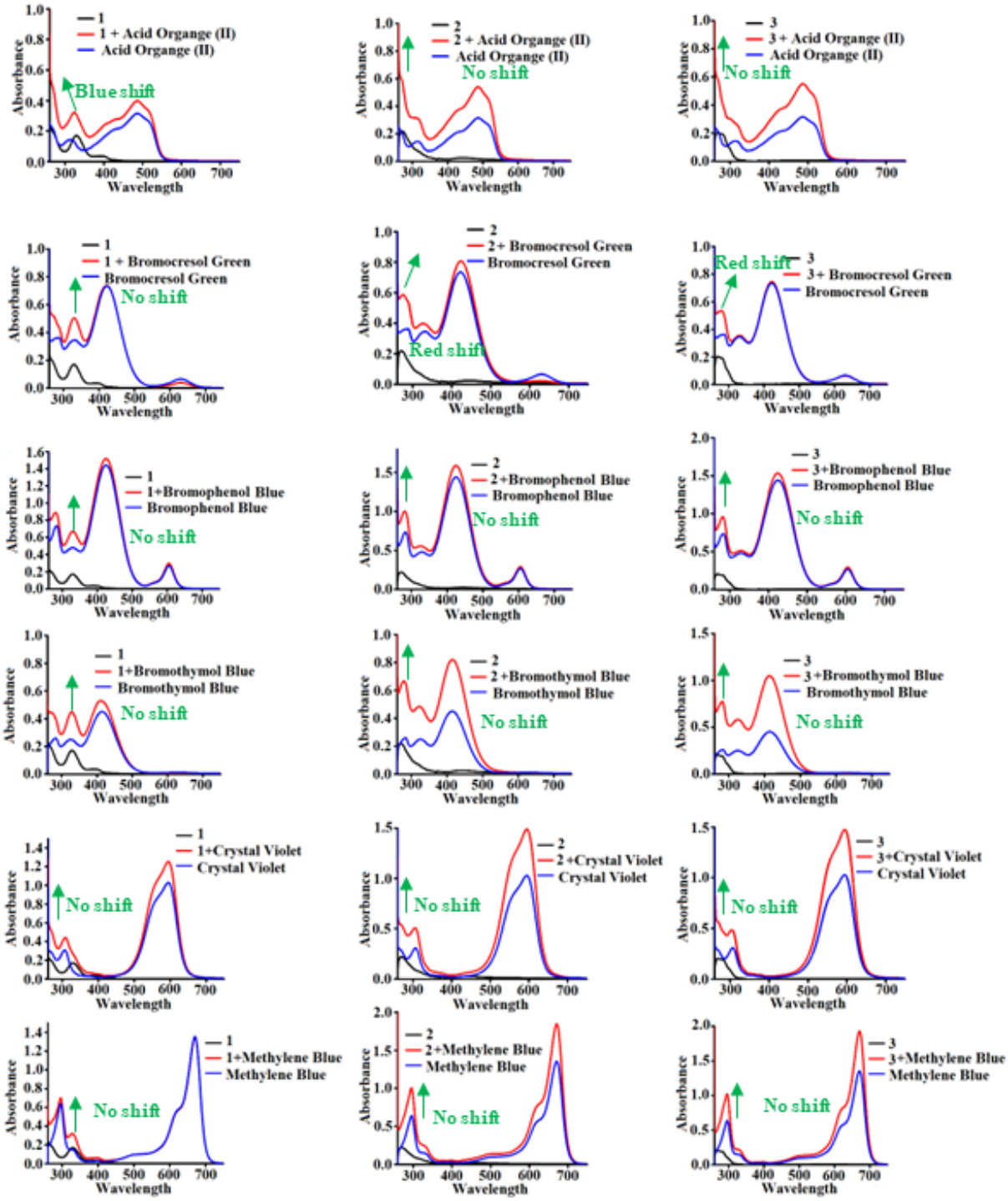

Figure 11. Sensing ability were examined by UV-Visible spectroscopy displaying a net blue shift of ~6 nm of Ni^{II} complex in presence of Acid orange (II) dye; a net red shift of ~5 nm of Cu^{II} complex in presence of bromo cresol green dye and a net red shift of ~9 nm of Zn^{II} complex in presence of Bromo cresol green dye.

However, the intensity of absorption bands of a majority of guest dyes are found to be increases during the interactions with selected hosts **1-3** (Figure 11). Our macrocycles are

found to effectively increases the absorption efficiency via the host-enhanced intramolecular charge transfer (ICT) effect/ electronic transitions.[28]

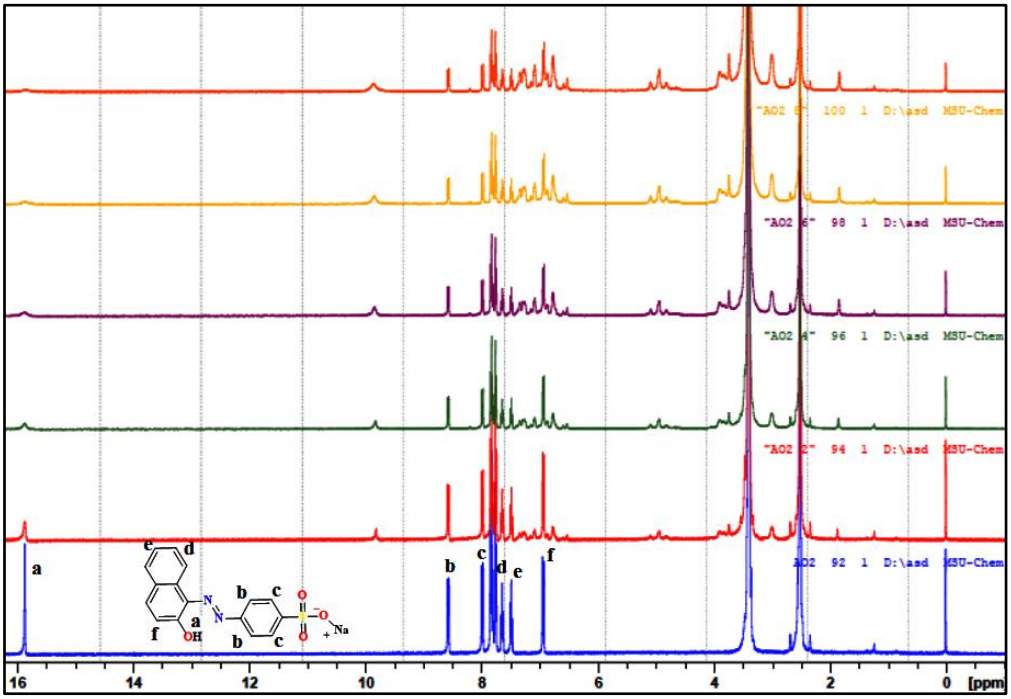

Figure 12. Complete ^{1}H NMR (400 MHz, 293K) spectra recorded during titration of G-1 (Acid Orange (II); 10 mM) with addition of molar equivalents of H-1 (Ni(II)-dithiocarbamate macrocycle 1; i) 0; ii) 0.2; iii) 0.4; iv) 0.6; v) 0.8; vi) 1.0 in DMSO-*d6*.

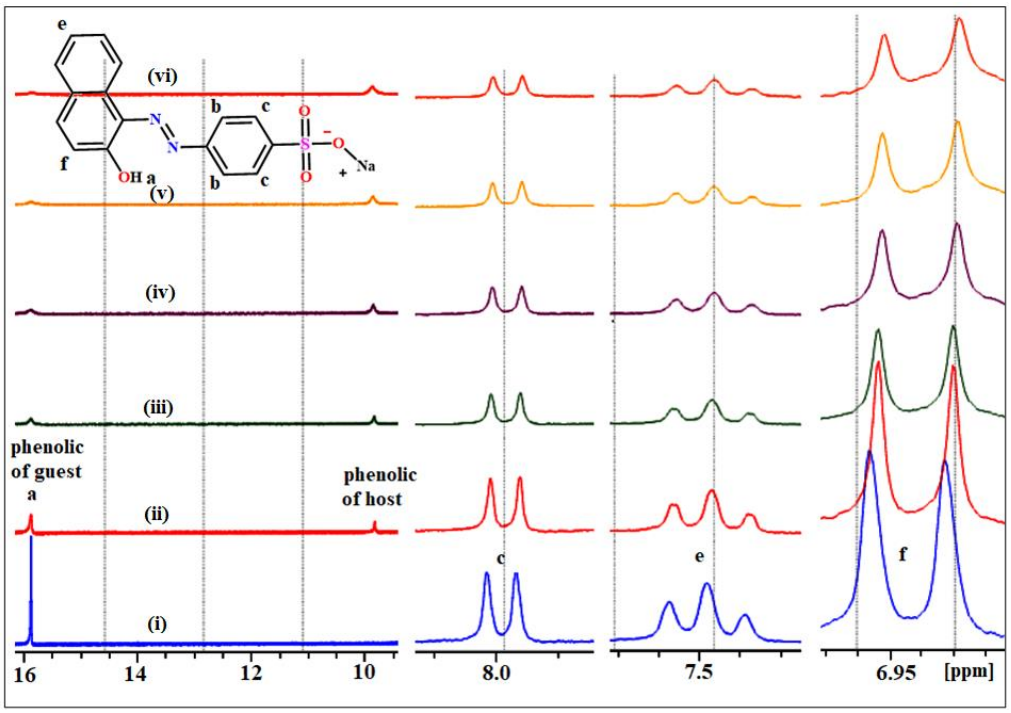

Figure 13. Partial ^{1}H NMR spectra (400 MHz, 293K) of G-1 (Acid Orange II; 10 mM) with addition of molar equivalents of H-1 (Ni(II)-dithiocarbamate macrocycle 1; i) 0; ii) 0.2; iii) 0.4; iv) 0.6; v) 0.8; vi) 1.0 in DMSO-*d6*.

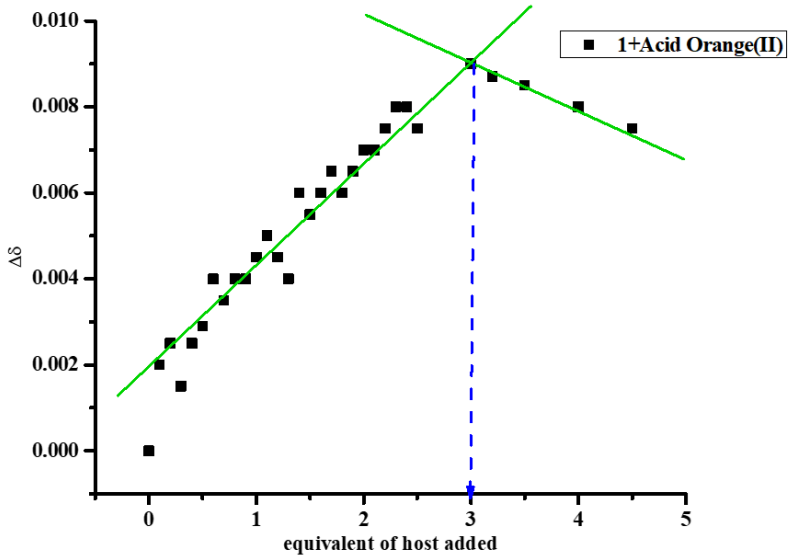

Figure 14. Stochiometric determination (3:1) of H-1 and Acid Orange II (G-1) by monitoring one of aromatic ^{1}H signal (6.95 ppm).

The binding efficacy of the diamagnetic Ni(II)-dithiocarbamate macrocycles **1** towards G-1 was further explored by using ^{1}H NMR titration techniques. The full range of the NMR spectra obtained during the titration is summarized in the supporting information (Figure 12) whereas the partial ^{1}H NMR spectra displaying the affected NMR signals during the addition of molar equivalents of H-1 into 10 mM solution of G-1 in DMSO-*d6* is shown in Figure 13. A careful evaluation of the spectral data reveals that one G-1 molecule is interacting with three H-1 molecules simultaneously. The broadening and downfield shifting of the phenolic signal of H-1 (Figure 13) indicate its involvement in the hydrogen bonding interaction with the potential sites of G-1. Further, the gradual downfield shifting and disappearance of phenolic signal of G-1 suggests its interaction with potential Lewis acidic metal centers of H-1. Interestingly, a substantial up-field shifting of aromatic signals (phenyl and naphthyl) of G-1 signifies the engagement of sulphonyl group in the coordination with Lewis acidic metal centers of H-1, making more electron-rich aromatic groups through M→L back donation. The stochiometric determination of H-1 and Acid Orange (II) (G-1), monitoring by the gradual shifting in one of aromatic ^{1}H signal (6.95 ppm) reveals the formation of 3:1 host-guest complex between H-1 and G-1. (Figure 14) In general, the presence of Lewis acidic metal centers, hydrophobic cavity and several polar substituents at the peripheral positions playing a crucial in the recognition of some of these hazardous dyes by our macrocycles. The hydrophobic, electrostatic and π–π stacking interactions between the host and a guest are apparently the driving forces in facilitating host-guest interactions. The

study provides a novel strategy to construct and utilize inorganic supramolecular macrocyclic systems based on dithiocarbamate for binding/ sensing of organic pollutants.

3.5 Conclusions

In conclusion, a new series of 32-membered homobimetallic dithiocarbamate macrocyclic complexes [M(II)$_2$-μ^2-bis-{κ^2S^S-$S_2CN(R)CH_2C_6H_3(OH)\}_2CH_2$] (R = 2-thiophenylethyl; Ni(II) **1**, Cu(II) **2**, Zn(II) **3;** R = cyclohexyl; Ni(II) **4**, Cu(II) **5**, Zn(II) **6**) were competently synthesized through single pot reaction involving 4,4'-methylenebis-2-((2-thiophen-2-yl)ethylamino)methylphenol (**H_2L^1**) or 4,4'-methylenebis-2-(cyclohexylamino)methylphenol (**H_2L^2**), CS_2 and transition metal ions. A number of analytical tools and density functional theory calculations were used to verify the composition and purity of the products.

Notably, the analysis of single crystal X-ray diffraction (SCXRD) data of Ni(II)-dithiocarbamate macrocyclic complex **1** reveals that complex **1** has the potential to form a fascinating 3D supramolecular structure possessing multiple opening of dimension: ~ 8.890 × 35.213 $Å^2$ in the solid state which opens a scope for macrocyclic complex **1** and its analogues to be investigated as a potential host in the host-guest supramolecular chemistry to sense/ bind hazardous organic dyes. Evidently, Ni(II)-dithiocarbamate macrocyclic complex **1** shown the ability to sense Acid Orange (II) selectively with considerable blue shifting of absorption bands whereas Cu(II) / Zn(II)-dithiocarbamate macrocyclic complexes **2** and **3** have shown the ability to sense Bromocresol green, selectively with significant red shifting of absorption bands. The ^{1}H NMR titration study reveals the formation of 3:1 host-guest stochiometric complex between **1** and Acid Orange (II) (G-1).

The presence of Lewis acidic metal centers, hydrophobic cavity and several polar substituents at the peripheral positions in our macrocycles are found to be crucial in the recognition as a potential host to sense/ bind hazardous organic dyes. The main driving forces in facilitating host-guest interactions are apparently hydrophobic, electrostatic and π–π stacking interactions between the host and guest. The present study exposes a new strategy to construct and utilize new homobimetallic dithiocarbamate macrocyclic complexes for binding/ sensing of organic pollutants.

3.6 References

[1] D. O. Oyeniran, T. O. Sogbanmu, T. A. Adesalu, *Ecotoxicol. Environ. Saf.* **2021,** *212,* 111982.

[2] V. Chandanshive, S. Kadam, N. Rane, B. H. Jeon, J. Jadhav, S. Govindwar, *Chemosphere.* **2020,** *252,* 126513.

[3] K. G. Akpomie, J. Conradie, *Ecotoxicol. Environ. Saf.* **2020**, *201*, 110825.

[4] A. Mudhoo, D. L. Ramasamy, A. Bhatnagar, M. Usman, M. Sillanp¨a¨a, *Ecotoxicol. Environ. Saf.* **2020,** *197,* 110587.

[5] (a) K. T. Chung, *Mutat. Res. Rev. Genet. Toxicol.* **1983,** *3,* 269; (b) M. A. S. Jiku, A. Singha, M. Faruquee, M. A. Rahaman, M. A. Alam, M. Ehsanullah, *Acta Ecol. Sin.* **2021,** *41 (4),* 358.

[6] A. M. Elgarahy, K. Z. Elwakeel, S. H. Mohammad, G. A. Elshoubaky, *Clean. Eng. Technol.* **2021**, *4,* 100209.

[7] S. Ao, T. Zayed, *Environ. Res.* **2022**, *203*, 111609.

[8] (a) T. A. Arica, M. Kuman, O. Gercel, E. Ayas, *Chem. Eng. Res. Des.* **2019,** *141,* 317; (b) D. Liu, J. Yuan, J. Li, G. Zhang, *ACS Omega.* **2019**, *4,* 12680.

[9] A. Islam, S. H. Teo, Y. H. Taufiq-Yap, C. H. Ng, D. V. N. Vo, M. L. Ibrahim, M. M. Hasan, M. A. R. Khan, A. S. Nur, M. R. Awual, *Resour. Conserv. Recycl.* **2021**, *175,* 105849.

[10] (a) S. Samsami, M. Mohamadizaniani, M. H. Sarrafzadeh, E. R. Rene, M. Firoozbahr, *Process Saf. Environ. Prot.* **2020**, *143*, 138; (b) C. E. Onu, B. N. Ekwueme, P. E. Ohale, C. P. Onu, C. O. Asadu, C. C. Obi, K. T. Dibia, O. O. Onu, J. Hazard. Mater. **2023**, *9*, 100224.

[11] (a) R. Kishor, D. Purchase, G. D. Saratale, R. G. Saratale, L. F. R. Ferreira, M. Bilal, R. Chandra, R. N. Bharagava, *J. Environ. Chem. Eng.* **2021**, *9,* 105012; (b) V. Katheresan, J. Kansedo, S. Y. Lau, *J. Environ. Chem. Eng.* **2018**, *6 (4),* 4676.

[12] (a) L. L. Coria-Oriundo, F. Battaglini, S. A. Wirth, *Ecotoxicol. Environ. Saf.* **2021,** *217,* 112237; (b) N. Asses, L. Ayed, N. Hkiri, M. Hamdi, *BioMed. Res. Int.* **2018**.

[13] (a) Z. Y. Bai, Q. Yang, J. L. Wang, *Int. J. Environ. Sci. Technol.* **2016,** *13*, 483; (b) Q. Dai, Z. Zhang, T. Zhan, Z.-T. Hu, *J. Chen, ACS Omega*. **2018**, *3*, 6506; (c) S. Shokrollahzadeh, M. Abassi and M. Ranjbar, *Environ. Eng. Res.* **2019**, *24*, 513; (d) A. D. Bokare, R. C. Chikate, C. V. Rode K. M. Paknikar, *Environ. Sci. Technol.* **2007,** *41,* 7437; (e) S. Zhang, H. Ren, K. Fu, W. Cheng, D. Wu, C. Luo, S. Jiang, J. Li M. Zhang, *Front. Energy Res.* **2022**, *9,* 1; (f) R. Rajesh, E. Sujanthi, S. S. Kumar and R. Venkatesan, *Phys. Chem. Chem. Phys.* **2015**, *17*, 11329; (g) S. Krishna, P. Sathishkumar, N. Pugazhenthiran, K. Guesh,

R. V. Mangalaraja, S. Kumaran, M. A. Gracia-Pinilla, S. Anandan, *RSC Adv.* **2020**, *10*, 16473; (h) B. Rodr´ıguez-Cabo, I. Rodr´ıguez-Palmeiro, R. Corchero, R. Rodil, E. Rodil, A. Arce, A. Soto, *Water Sci. Technol.* **2016**, *75*, 128; (i) H. T. Van, V. H. Hoang, T. C. Luu, T. L. Vi, L. T. Quynh Nga, G. S. Ivan Jimenez Marcaida, T. -T. Pham, *RSC Adv*., **2023**, *13*, 28753.

[14]. T. A. Aragaw, F. M. Bogale, *Front. Environ. Sci.* **2021,** *9*, 764958.

[15]. (a) R. N. Dsouza, U. Pischel, W. M. Nau, *Chem. Rev.* **2011**, *111*, 7941; (b) H. Bakirci, A. L. Koner, W. M. Nau, *J. Org. Chem.* **2005**, *70*, 9960. (c) J. Cui, V. D. Uzunova, D.S. Guo, K. Wang, W. M. Nau, Y. Liu, *Eur. J. Org. Chem.* **2010**, 1704. (d) B. D. Wagner, S. J. Fitzpatrick, *J. Inclusion Phenom. Macrocyclic Chem.* **2000**, *38*, 467. (e) K. N. Baglole, P. G. Boland, B. D. Wagner, *J. Photochem. Photobiol.* **2005**, *173*, 230. (f) L. S. Yakimova, D. N. Shurpik, L. H. Gilmanova, A. R. Makhmutova, A. Rakhimbekova, I. I. Stoikov, *Org. Biomol. Chem.* **2016**, *14*, 4233. (g) L. Thurakkal, P. Nanjan, M. Porel, *Scientific Reports,* **2022**, *12*, 4815.

[16] (a) R. Kadu, K. Kolte, C. Savani, S. S. Zade, A. A. Isab, A. K. Singh, V. K. Singh, *Journal of Molecular Structure.* **2023**, *1287,* 135657; (b) V. K. Singh, V. Pillai; S. K. Patel, L. Buch, *ChemistrySelect.* **2019**, *4*, 8689; (c) V. Pillai, S. K. Patel, L. Buch, V. K. Singh, *Appl. Organomet. Chem.* **2018**, *32*, e4559; (d) V. Pillai, L. Buch, A. Desai, V. K. Singh, *ChemistrySelect*. **2017**, *2*, 11581. (e) V. Pillai, R. Kadu, L. Buch, V. K. Singh, *ChemistrySelect*. **2017**, *2*, 4382; (f) R. Kadu, H. Roy, V. K. Singh, *Appl. Organometal. Chem.* **2015**, *29*, 746.

[17] (a) A. Jana, S. Bhowmick, S. Kaur, H. K. Kashyap, N. Das, *Dalton Trans.* **2017**, *46*, 1986; (b) Lee, S. M.; Tiekink, E. R. T. *Inorganics.* **2021**, *9*, 7; (c) I. Rojas-León, H. Alnasr, K. Jurkschat,; Vasquez-Ríos, M. G.; Gómez-Jaimes, G.; Höpfl, H.; Hernández-Ahuactzí, I. F.; Santillan, R. *Organometallics.* **2019**, *38*, 2443; (d) Torres-Huerta, A.; Höpfl, H.; Tlahuext, H; I. F. Hernández-Ahuactzi, M. Sánchez, R. Reyes-Martínez, D. Morales-Morales, *Eur. J. Inorg. Chem.* **2013**, 61; (e) A. Torres-Huerta, J. Cruz-Huerta, H. Höpfl, L. G. Hernández-Vázquez, J. Escalante-García, A. Jiménez-Sánchez, R. Santillan, I. F. Hernández-Ahuactzi, M. Sánchez, *Inorg. Chem.* **2016**, *55*, 23**,** 12451; (f) J. Cruz-Huerta, M. Carillo-Morales, E. Santacruz-Juárez, I. F. Hernández-Ahuactzi, J. Escalante-García, C. Godoy-Alcantar, J. A. Guerrero-Alvarez, H. Höpfl, H. Morales-Rojas, M. Sánchez, *Inorg. Chem.* **2008**, *47*, 9874; (g) P. Selvaganapathi, S. Thirumaran, S. Ciattini, **2019**, *33*, e5089.

[18] (a) R. Kadu, V. Pillai, V. Amrit, V. K. Singh, *RSC Adv.* **2015**, *5*, 106688; (b) P. D. Beer, N. G. Berry, A. R. Cowley, E. J. Hayes, E. C. Oates, W. W. H. Wong, *Chem. Commun.* **2003**,

2408; (c) J. Cookson, P. D. Beer, *Dalton Trans.* **2007**, 1459; (d) J. Cookson, E. A. L. Evans, J. P. Maher, C. J. Serpell, R. L. Paul, A. R. Cowley, M. G. B. Drew, P. D. Beer, *Inorg. Chim. Act.* **2010**, *363*, 1195; (d) J. H. Lamm, P. Niermeier, A. Mix, J. Chmiel, B. Neumann, H. G. Stammler, N. W. Mitzel, Angew. *Chem. Int. Ed.* **2014**, *53*, 1; (e)A. Torres-Huerta, J. Cruz-Huerta, H. Höpfl, L. G. Hernández-Vázquez, J. Escalante-García, A. Jiménez-Sánchez, R. Santillan, I. F. Hernández-Ahuactzi, M. Sánchez, *Inorg. Chem*. **2016**, *55*, 12451; (f) J. C. Sarker, G. Hogarth, *Chem. Rev.* **2021**, *121*, 10, 6057; (g) B. C. Tzeng, C. L. Wu, J. W. Hung, S. Y. Chienb, G. H. Lee, *Dalton Trans.* **2022**, *51*, 16973.

[19] (a) S. K. Patel, K. Kolte, C. J. Savani, P. Raghavaiah, D. Dave, A. A. Isab, D. Mistry, D. Suthar, V. K. Singh, *Inorganica Chimica Acta,* **2022,** *543,* 121139; (b) E. Sonbati, A. Z. *Synth. React. Inorg. Met.-Org. Chem*. **1991**, *21*, 203; (c) K. S. Siddiqi, Nami, S. A. A. Lutfullah, Y. Chebude, *J. Braz. Chem. Soc.* **2006**, *17*, 107; (d) F. Bensebaa, Y. Zhou, A. G. Brolo, D. E. Irish, Y. Deslandes, E.; Ellis, T. H. Kruus, *Spectrochim. Acta*. **1999**, *55A*, 1229.

[20] (a) M. Rico, J. M. Orza, J. Morcillo, *Spectrochim.* **1965**, Acta 21, 689; (b) F. Alakhras, R. Holze, *Synth. Met.* **2007**, *157*,109; (c) K. Kolte, V. K. Singh, S. K. Patel, *J. Mol. Struct.* **2024,** *1300,* 137165.

[21] P. D. Beer, A. G. Cheetham, M. G. B. Drew, O. Danny Fox, J. Elizabeth Hayes, T. D. Rolls, *Dalton Trans*. **2003**, *4*, 603.

[22] M. J. Frisch, G. W. Trucks, H. B. Schlegel, G. E. Scuseria, M. A. Robb, J. R. Cheeseman, G. Scalmani, V. Barone, G. A. Petersson, H. Nakatsuji, X. Li, M. Caricato, A. V. Marenich, J. Bloino, B. G. Janesko, R. Gomperts, B. Mennucci, H. P. Hratchian, J. V. Ortiz, A. F. Izmaylov, J. L. Sonnenberg, D. Williams-Young, F. Ding, F. Lipparini, F. Egidi, J. Goings, B. Peng, A. Petrone, T. Henderson, D. Ranasinghe, V. G. Zakrzewski, J. Gao, N. Rega, G. Zheng, W. Liang, M. Hada, M. Ehara, K. Toyota, R. Fukuda, J. Hasegawa, M. Ishida, T. Nakajima, Y. Honda, O. Kitao, H. Nakai, T. Vreven, K. Throssell, J. A. Montgomery, Jr., J. E. Peralta, F. Ogliaro, M. J. Bearpark, J. J. Heyd, E. N. Brothers, K. N. Kudin, V. N. Staroverov, T. A. Keith, R. Kobayashi, J. Normand, K. Raghavachari, A. P. Rendell, J. C. Burant, S. S. Iyengar, J. Tomasi, M. Cossi, J. M. Millam, M. Klene, C. Adamo, R. Cammi, J. W. Ochterski, R. L. Martin, K. Morokuma, O. Farkas, J. B. Foresman, D. J. Fox, Gaussian, Inc., Wallingford CT, **2016**.

[23] GaussView, Version 6.1, Dennington, R.; Keith, T. A.; Millam, J. M. Semichem Inc., Shawnee Mission, KS, **2016**.

[24] (a) M. G. Vasquez-Rios, V. Reyes-Marquez, H. Hopfl, A. Torres-Huerta, J. Guerrero-Alvarez, M. Sanchez, I. F. Hernandez-Ahuactzi, K. Ochoa-Lara, A. Jimenez-Sanchez, R.

Santillan, *Eur. J. Inorg. Chem.* **2016**, 3429; (b) R. Kadu, K. Kolte, C. Savani, S. S. Zade, A. A. Isab, A. K. Singh, V. K. Singh, *J. Mol. Struct.* **2023**, *1287*, 135657; (c) V. K. Singh, R. Kadu, H. Roy, R. Pallepogu, S. M. Mobin, *Dalton Trans.* **2016**, *45*, 1443; (d) N. A. Celis, R. Villamil-Ramos, H. Hopfl, I. F. Hernandez-Ahuactzi, M. Sanchez, L. S. Zamudio-Rivera, V. Barba, *Eur. J. Inorg. Chem.* **2013**, 2912; (e) K. Gholivand, M. Rajabi, N. Dorosti, F. Molaei, *Appl. Organomet. Chem.* **2015**, *29*, 739.

[25] S. K. Patel, K. Kolte, C. J. Savani, P. Raghavaiah, D. Dave, A. A. Isab, D. Mistry, D. Suthar, V. K. Singh, *Inorg. Chim. Acta.* **2022**, *543*, 121139.

[26] P. Zheng, Z. Li, L. Tong, R. Lu, *J. Incl. Phenom. Macrocyl. Chem.* **2002**, *43*, 183.

[27] L. S. Yakimova, D. N. Shurpik, L. H. Gilmanova, A. R. Makhmutova, A. Rakhimbekov, I. I. Stoikov, *Org. Biomol. Chem.* **2016**, *14*, 4233.

[28] Y. Si, Q. Zhang, W. Jin, S. Yang, Z. Wang, D. Qu, *Dyes and Pigments.* **2020**, *173*, 107919.

3.7 Annexures

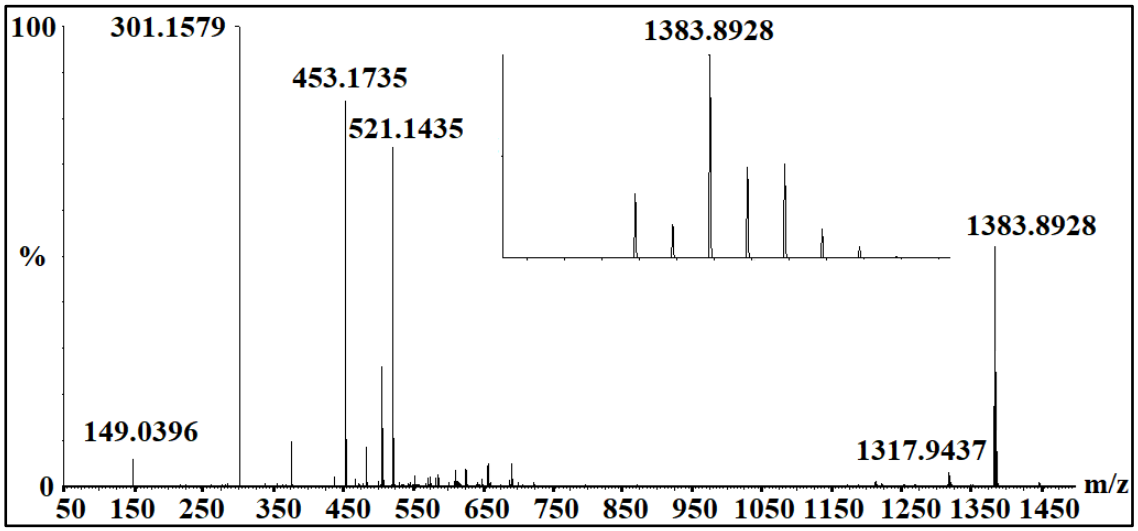

Annexure 1. HRMS of complex **2.**

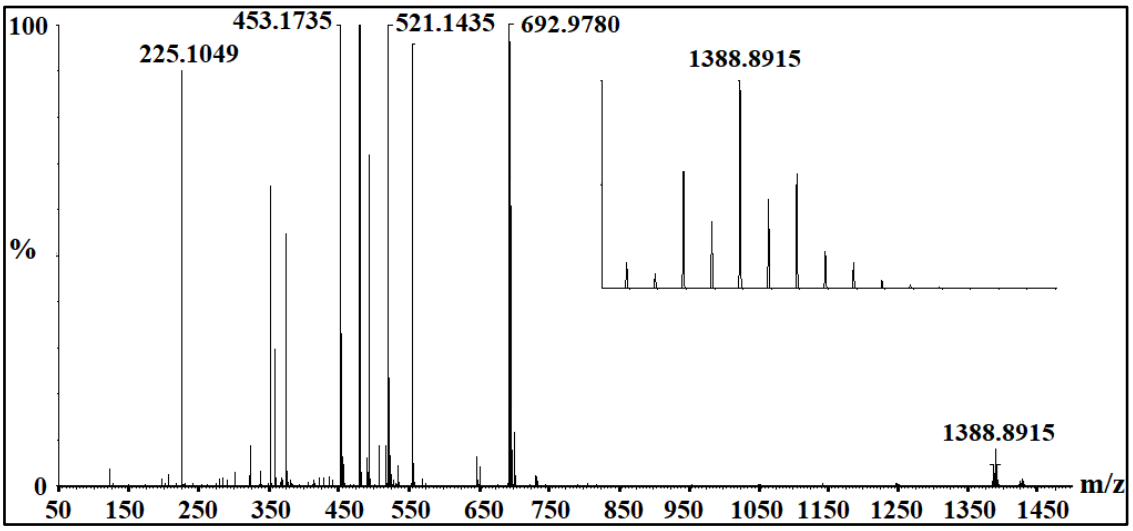

Annexure 2. HRMS of complex **3.**

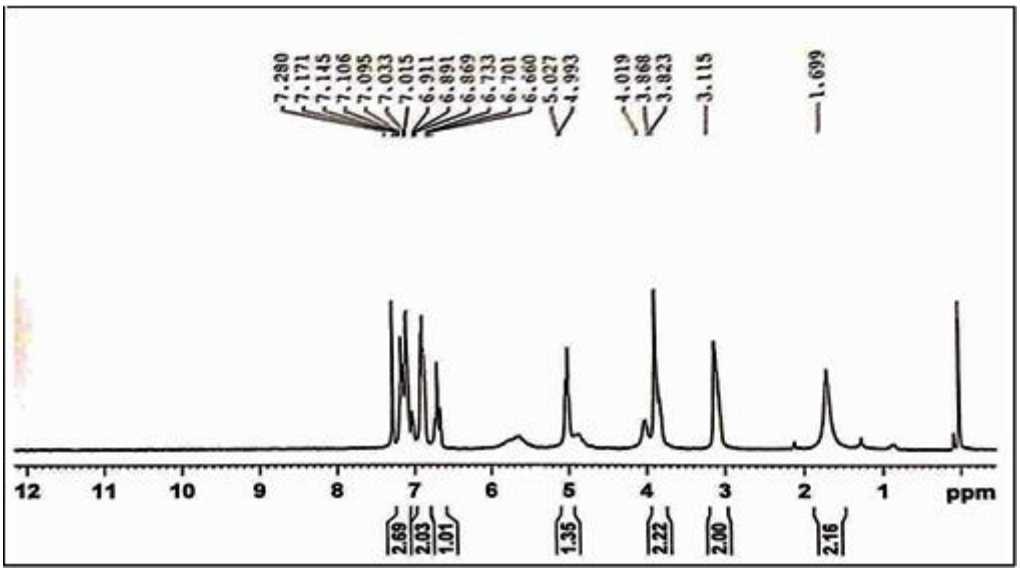

Annexure 3. ^{1}H NMR of complex **1**.

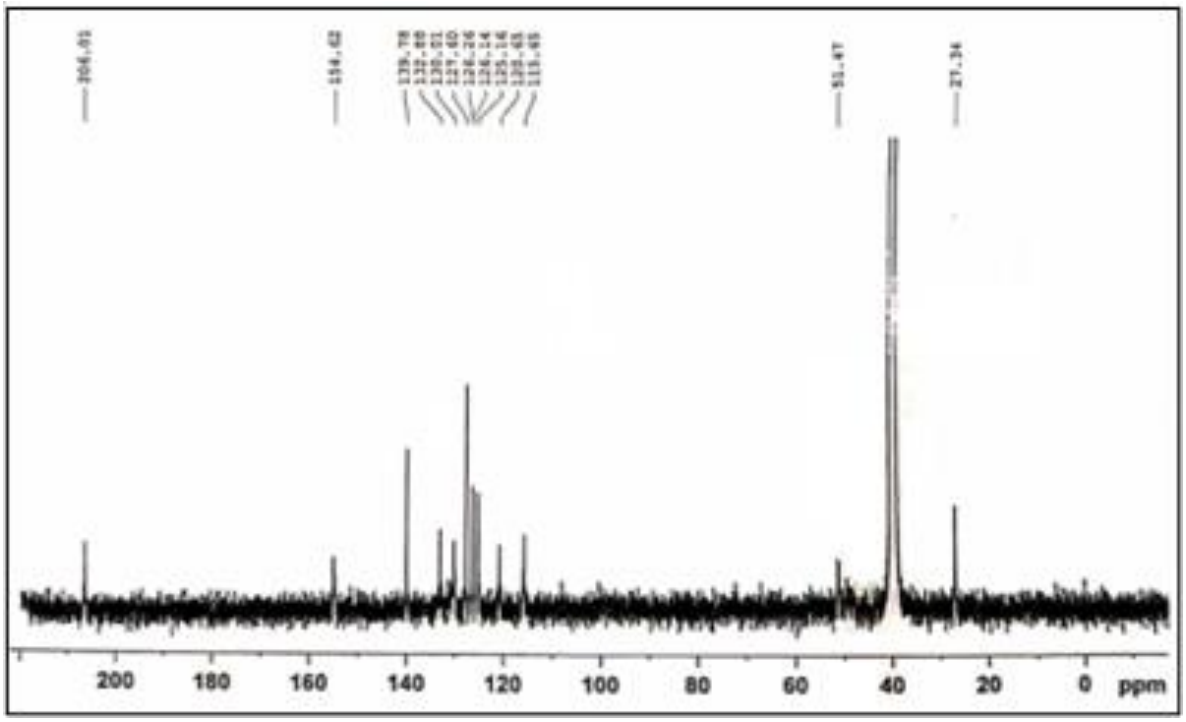

Annexure 4. ^{13}C NMR of complex **1**.

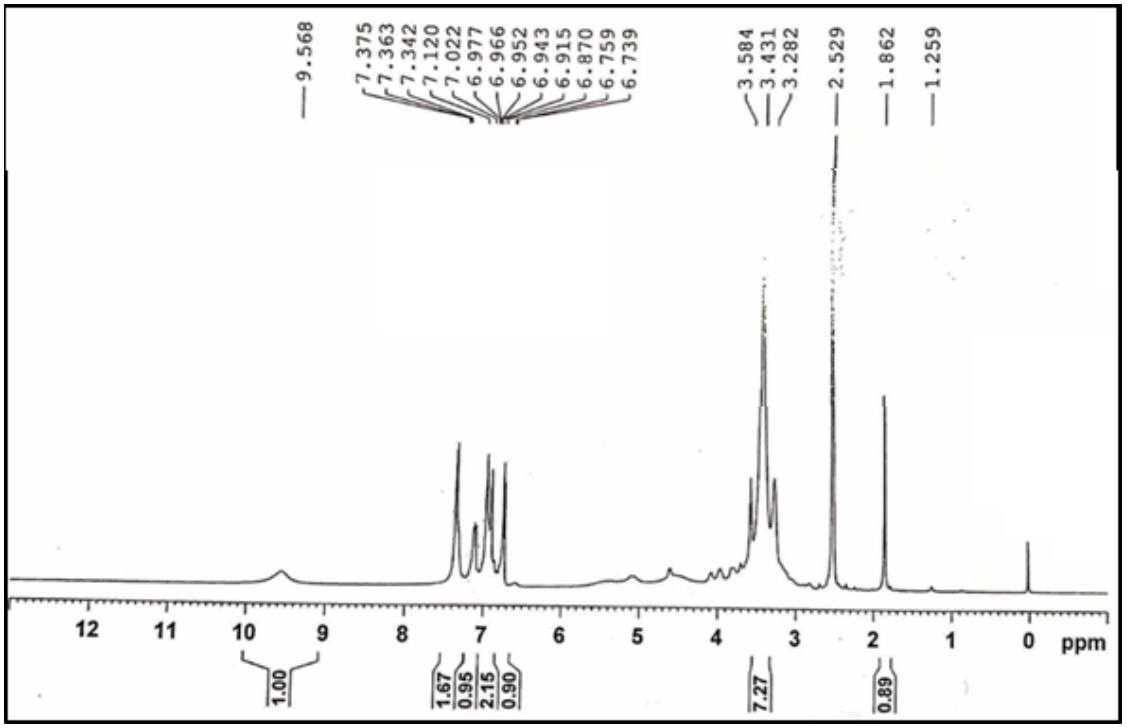

Annexure 5. ^{1}H NMR of complex **3.**

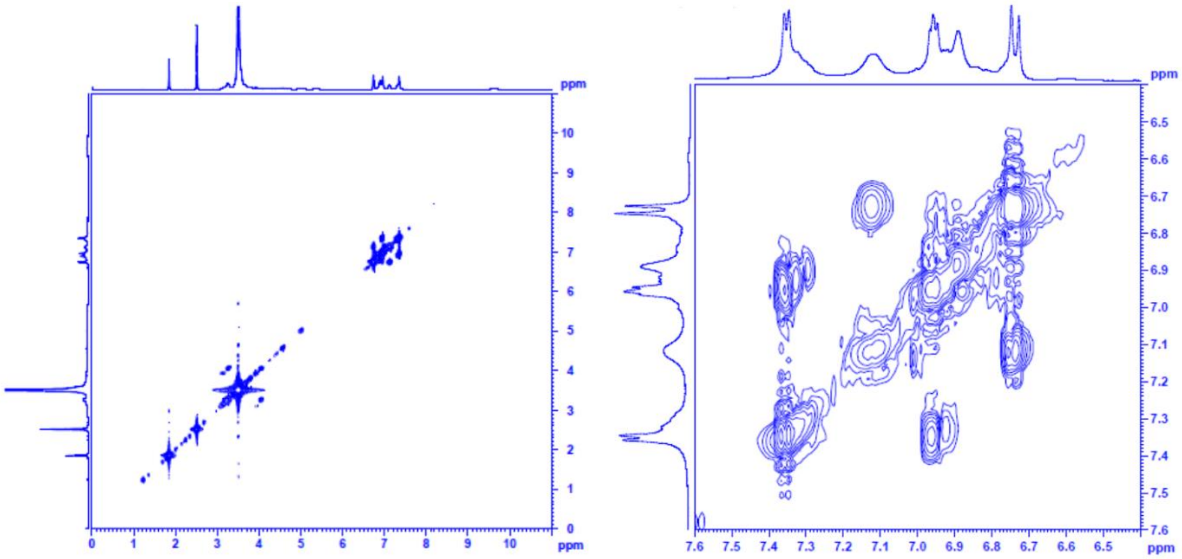

Annexure 6. COSY NMR spectrum of complex **3**.

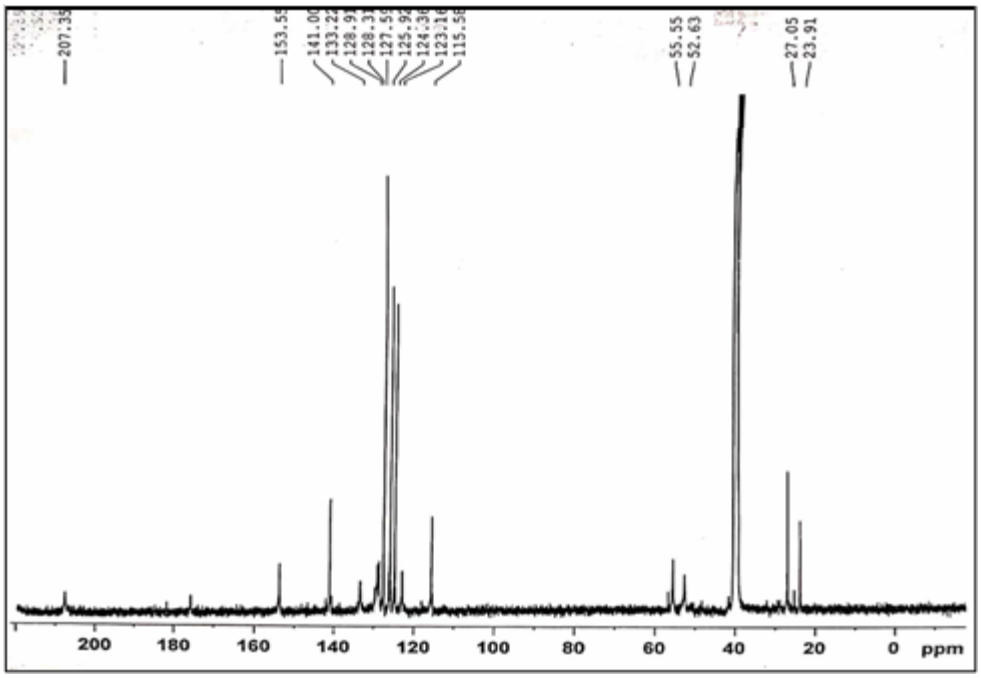

Annexure 7. ^{13}C NMR of complex **3.**

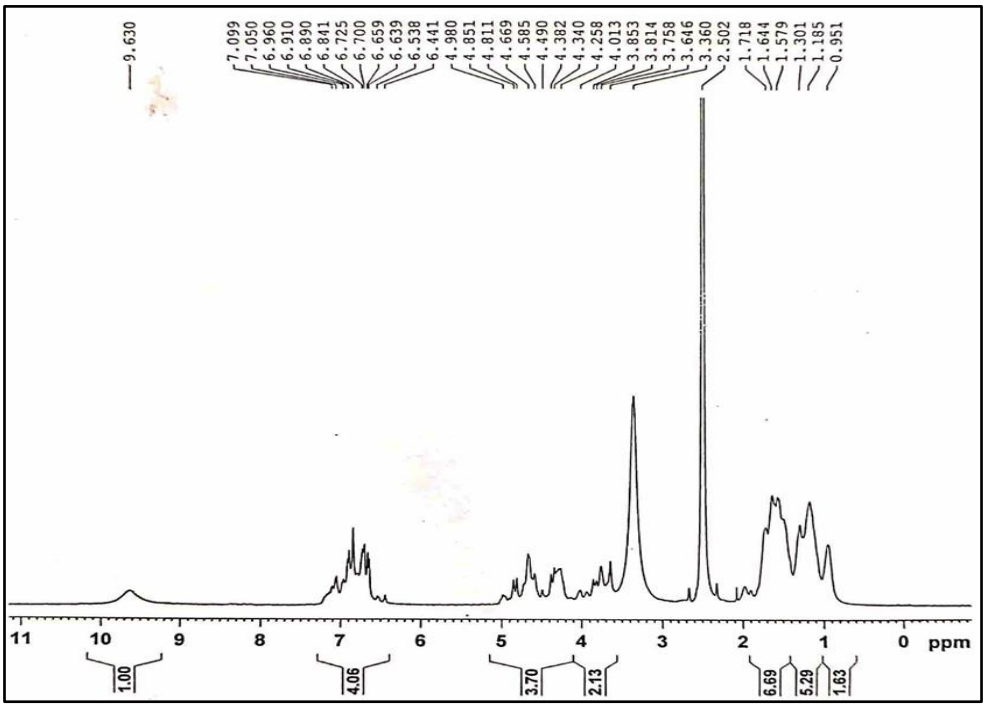

Annexure 8. complex **4**.

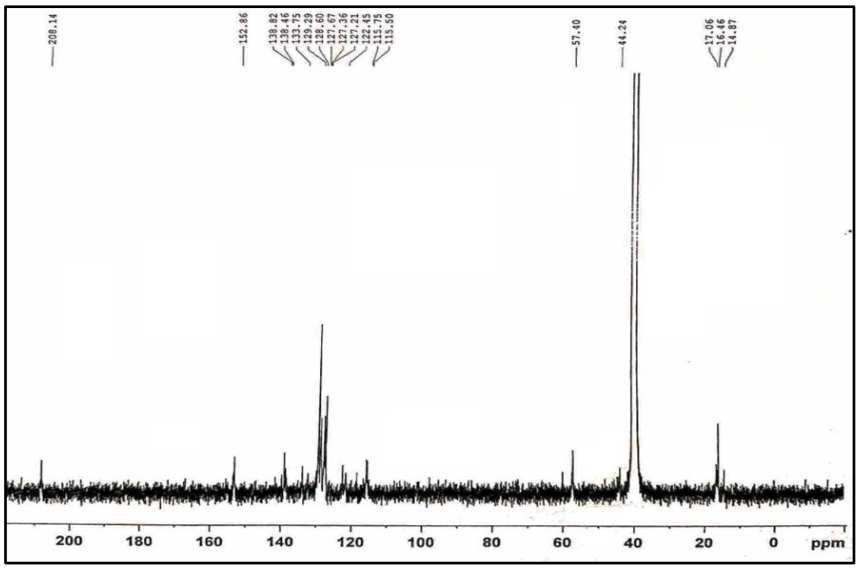

Annexure 9. ^{13}C NMR of complex **4**.

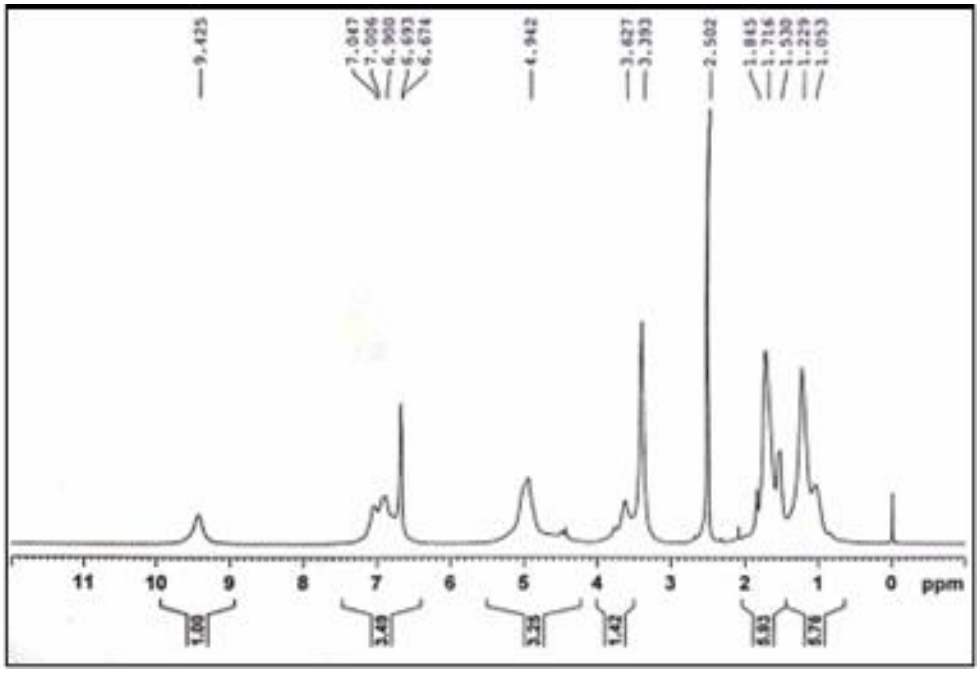

Annexure 10. ^{1}H NMR of complex **6**.

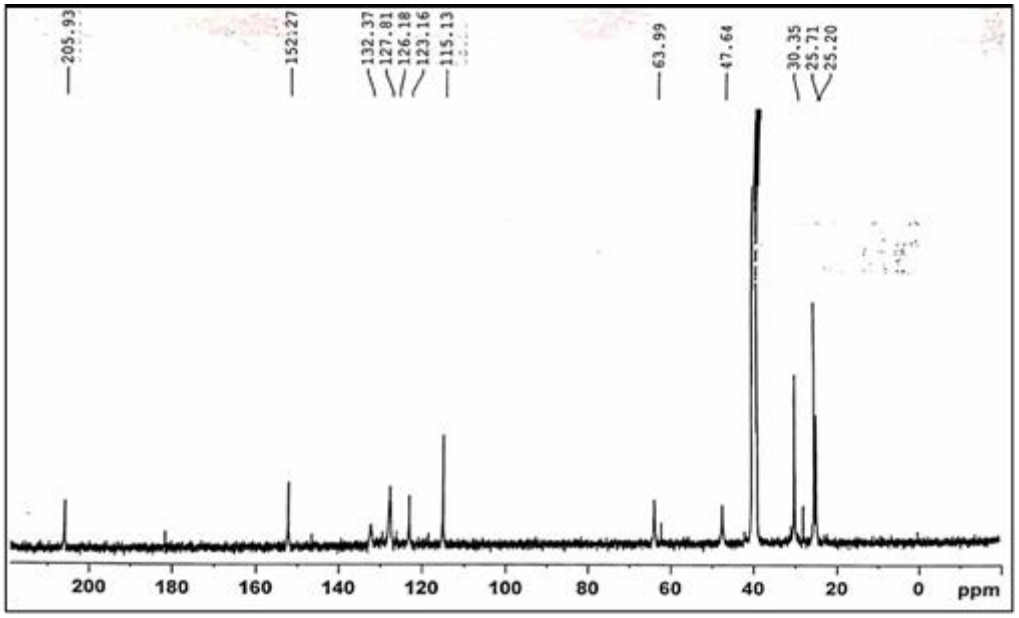

Annexure 11. ^{13}C NMR of complex **6**.

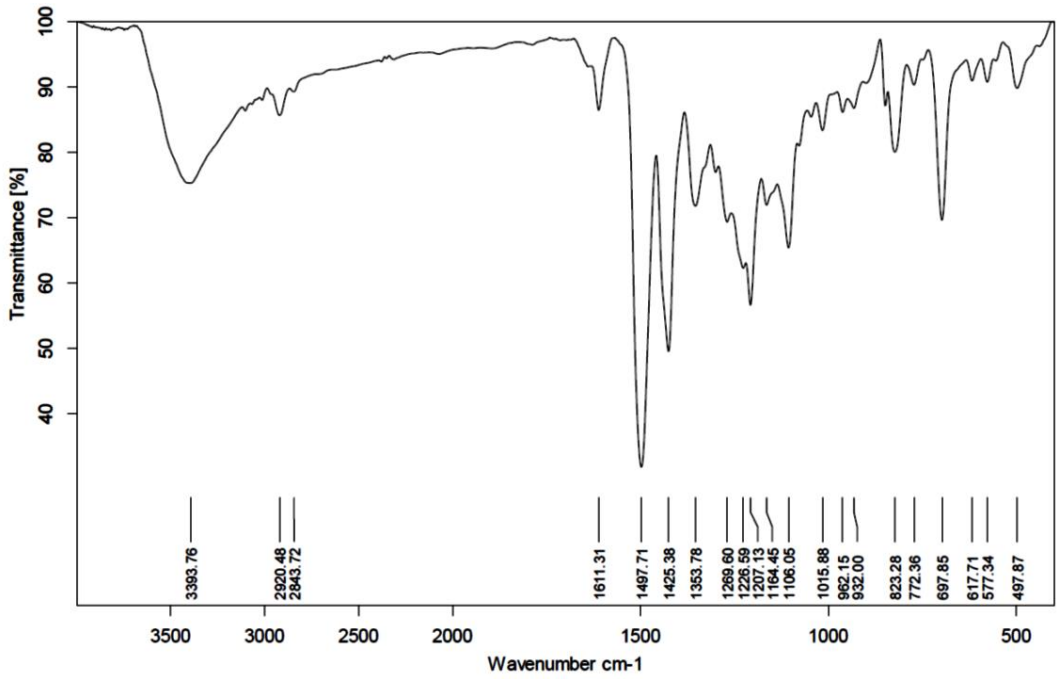

Annexure 12. FTIR spectrum of complex **1**.

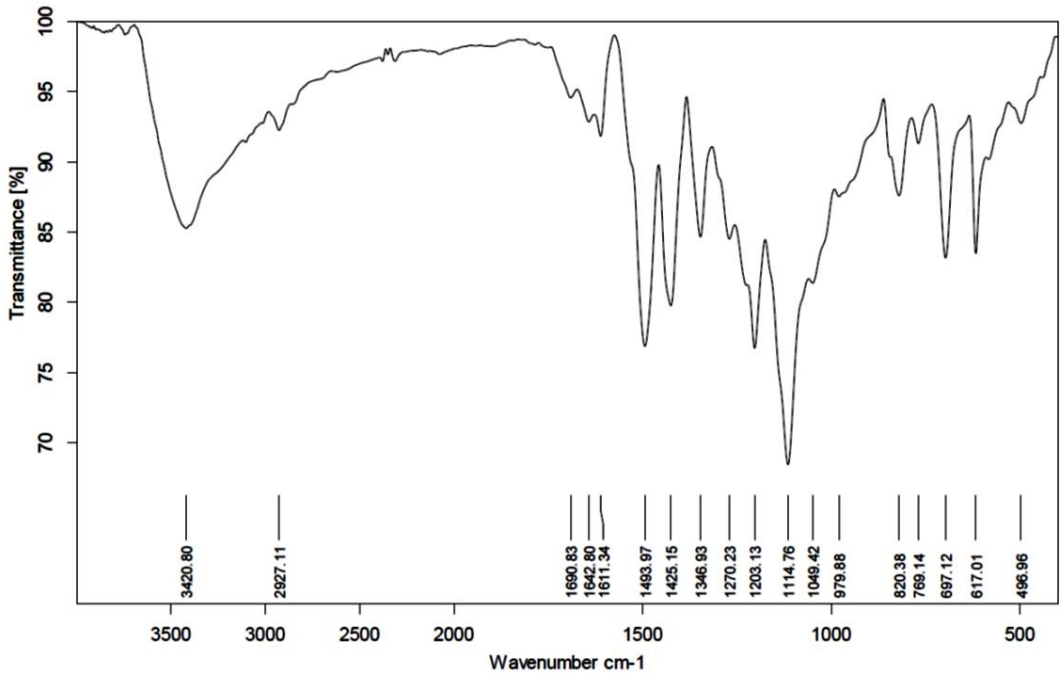

Annexure 13. FTIR spectrum of complex **2**.

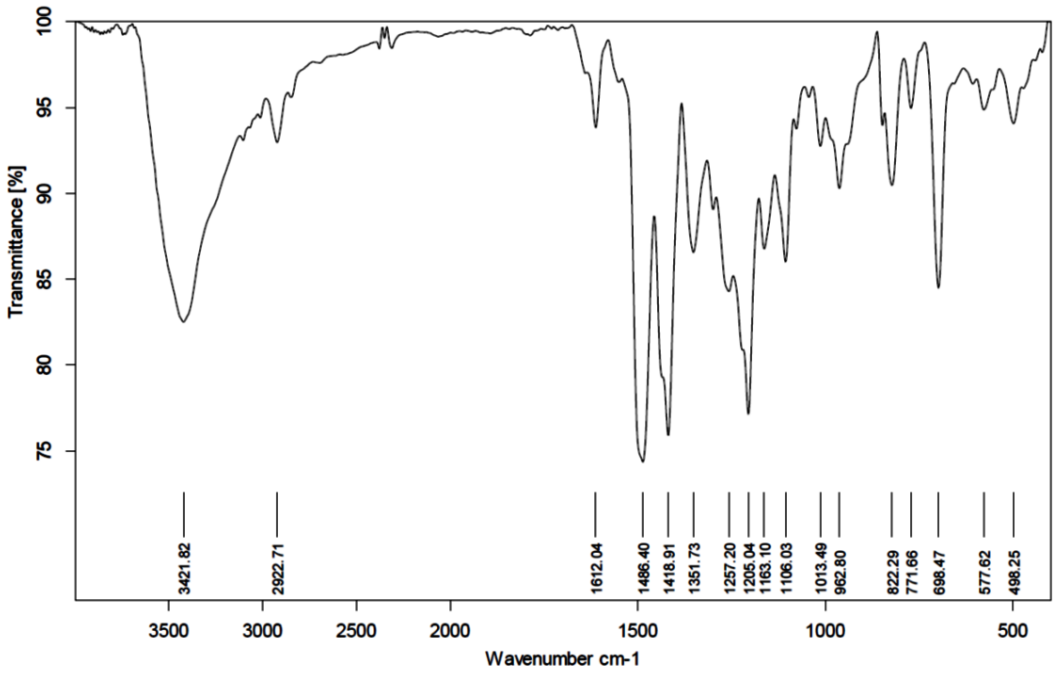

Annexure 14. FTIR spectrum of complex **3.**

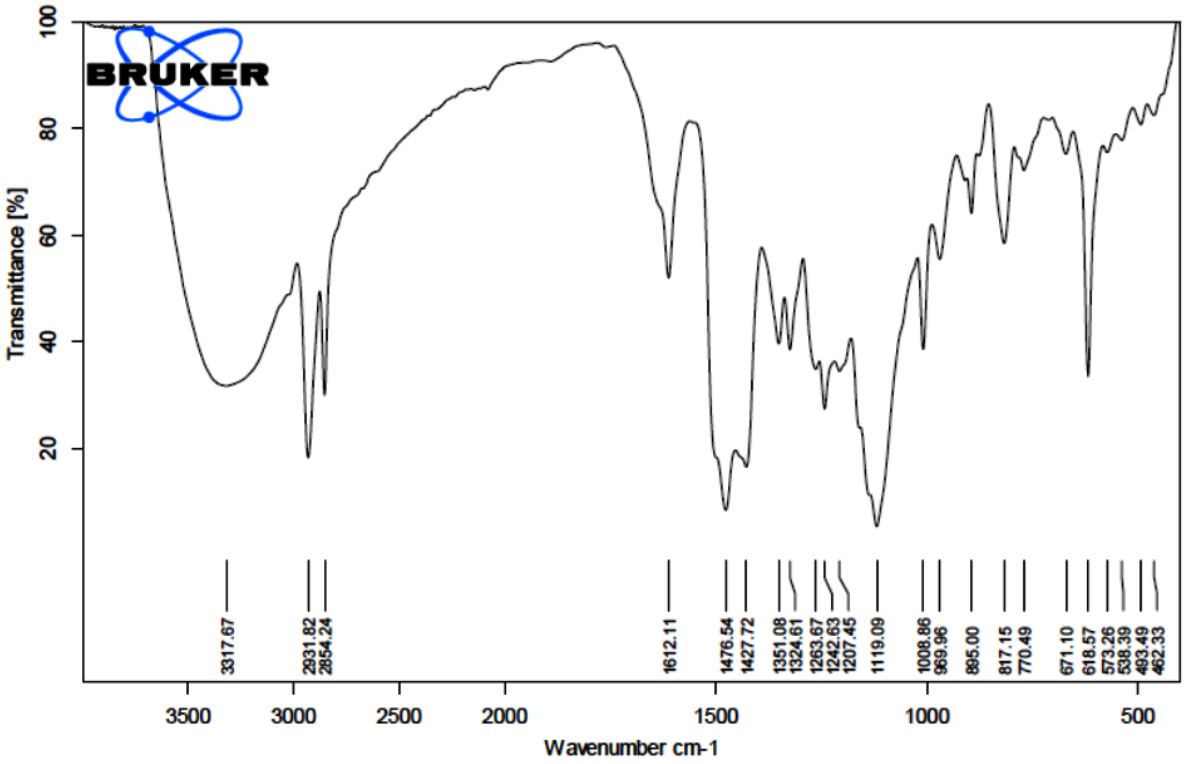

Annexure 15. FTIR spectrum of complex **4**.

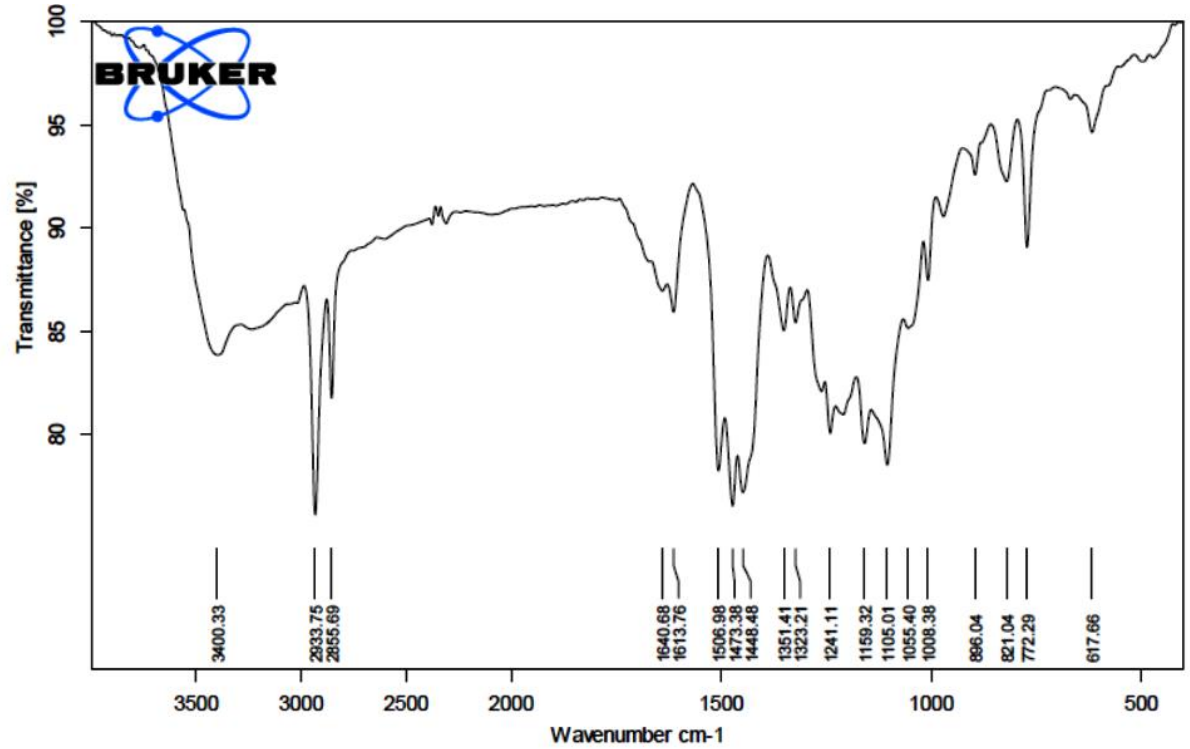

Annexure 16. FTIR spectrum of complex **5**.

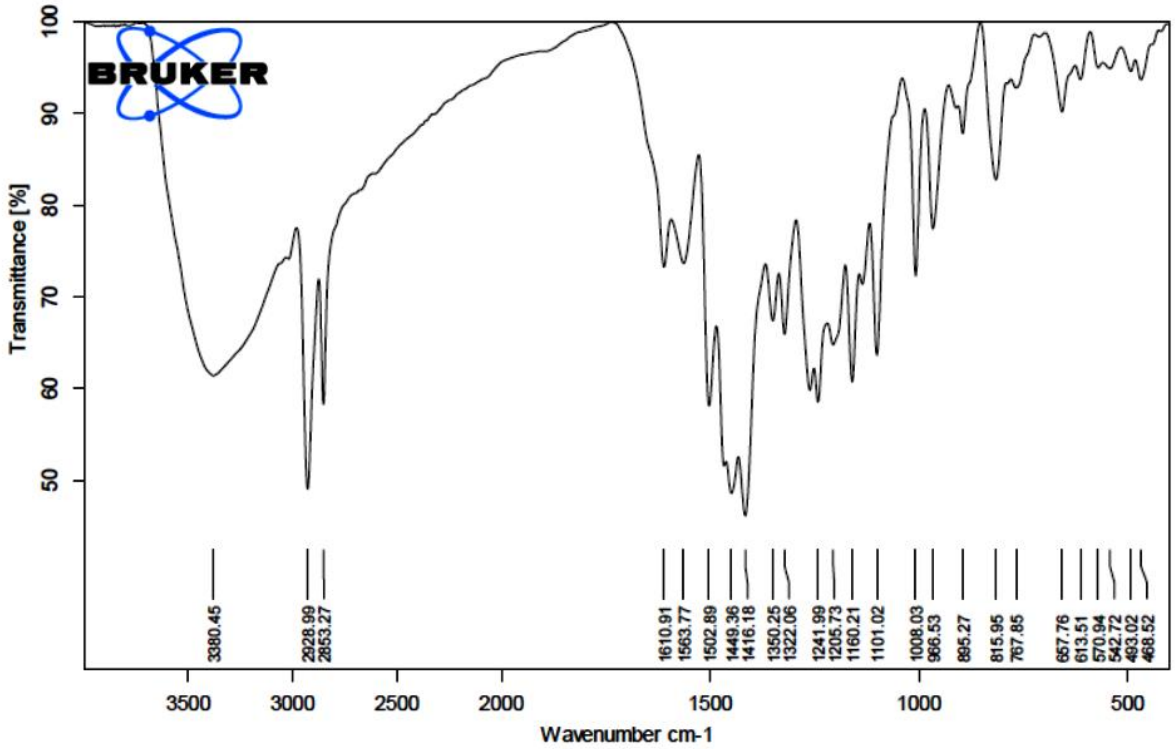

Annexure 17. FTIR spectrum of complex **6**.